Department of Physics and Astronomy

University of Heidelberg

Diploma thesis

in Physics

submitted by

Dominik Globig

born in Soest

2011

A Laser Cooled Lithium Beam Source for the Loading of a Magneto-Optical Trap in a Reaction Microscope

This diploma thesis has been carried out by Dominik Globig

at the

Max-Planck-Institut für Kernphysik

under the supervision of

Dr. Daniel Fischer

Zusammenfassung:

Am Max-Planck-Institut für Kernphysik (MPIK) wird im Rahmen des PRIOC-Projektes (**Pr**ecision studies on **I**on **C**ollisions) ein neues Experiment aufgebaut, bei dem ein Reaktionsmikroskop (Remi) mit einer magneto-optischen Falle (MOT) als Target zu einem sogenannten MOTRemi kombiniert wird. Dieser Aufbau soll in den Testspeicherring (TSR) des MPIK implementiert werden. Die weltweit einzigartige Kombination dieser drei modernen Techniken soll die kinematisch vollständige Untersuchung von Ion-Atom-Stößen in bisher unerreichter Detailliertheit und Auflösung ermöglichen. Im Rahmen dieser Arbeit wurde eine zweidimensionale magneto-optische Falle (2D-MOT) als Quelle für langsame Lithiumatome zum Laden der Target-MOT entwickelt und getestet. Diese Methode erlaubt einen sehr kompakten Aufbau und liefert einen kollimierten Strahl mit einem Fluss kalter Atome in der Größenordnung, die den höchsten bisher mit Laserkühlung erreichten Flüssen entspricht. Die Temperatur des atomaren Strahls liegt dabei im Bereich weniger Kelvin und ermöglicht es, den Strahl selbst als Target für impulsaufgelöste Stoßexperimente zu benutzen.

Abstract:

A new experiment is being built at the Max-Planck-Institut für Kernphysik (MPIK) within the PRIOC project (**Pr**ecision studies on **I**on **C**ollisions) where a reaction microscope (Remi) and a magneto-optical trap (MOT) as target are combined to a so called MOTRemi. This setup will be implemented into the ion storage ring 'Testspeicherring' (TSR) of the MPIK. The world-wide unique combination of these three state-of-the-art technologies shall enable to perform kinematically complete studies of ion-atom collision with unprecedented detail and resolution. In this thesis, a two-dimensional magneto-optical trap (2D-MOT) was developed and tested as a source of slow lithium atoms for the loading of the target MOT. This method allows a very compact setup and offers a collimated beam and a flux of cold atoms comparable to the highest fluxes achieved by using laser cooling. The temperature of the atomic beam was determined to be at the scale of a few Kelvin and, thus, it is already an adequate stand-alone target for momentum resolved experiments.

Contents

1 Introduction

The study of the interaction of ions with matter is a very old and historically important field in physics. Already in 1911, Rutherford examined the scattering of helium nuclei in a thin gold foil [Rut11]. By investigating the scattering profile of the α-particles, i.e. by studying differential cross sections, he set a milestone in understanding the atomic structure and two-body coulomb scattering dynamics. In the case of ion-impact ionization of atoms the theoretical description of the scattering process becomes substantially more difficult than in the case of two-body Rutherford scattering. Here, there are at least three particles explicitely involved: The projectile ion, the target core, and the ionized electron. For three or more particles, however, the (classical as well as quantum mechanical) equations of motion cannot be solved analytically anymore. Thus, the 'Few-Body Problem' can only be tackled applying theoretical approximations. Due to the rapid evolution in computer technology in the last decades, nowadays exact 'brute force' numerical methods can also be used in some cases (e.g. [RBIM99]). The first quantum-mechanical approach to describe the ion-impact induced ionization of atoms was developed by Bethe in the early 1930s [Bet30]. In his approximation the interaction between the projectile ion and the target atom is basically treated in the first perturbative order. This so-called 'First Born Approximation' is frequently used to date and very successful for swift ion-atom collions.

In the first quantitative experiments on ion-impact ionization only total cross sections were obtained. Already in the 1960s, more detailed studies have been performed exploiting electron spectroscopy (e.g [RJJ63]). However, kinematically complete experimts, i.e. investigations where the momenta of all involved particles are obtained, became only feasible after the development of so-called reaction microscopes and the COLTRIMS thechnique (cold target recoil ion momentum spectroscopy) (e.g. [UMD+97]). Only in 2001, the first fully differential cross sections (FDCS) on ion-impact ionization are reported [SMM+01]. Shortly thereafter, a detailed study of the three-dimensional FDCS [UMD+03b] for single ionization in

100 MeV/amu C^{6+}-He collisions revealed strong discrepancies to perturbative theoretical models. This surprinsing outcome triggered a lot of activity on the theoretical side. However, to date essentially all available theoretical approaches have considerable difficulties to reproduce experimental data (e.g. [MAM+10]).

Several explanations for these discrepancies have been discussed: The correlation of the electrons in the helium atom could affect the collision dynamics. These correlations have not yet been taken into account in theoretical calculations [FMS+03] and [FO04]. Also, multiple scattering processes have not been considered [SDN+07]. Furthermore, the experimental resolution is claimed to have a huge effect on the measured spectra. And a theoretical consideration of its effects is complex and cannot generally be accomplished [FOO06], [DNS07].

At the Max-Planck-Institut für Kernphysik (MPIK), a new experiment has been developed within the PRIOC (**Pr**ecision studies on **I**on **C**ollisions) project that will help to study the above discussed effects more closely. A reaction microscope (Remi) is combined with a magneto-optical trap (MOT), a so called MOTRemi. The MOTRemi will be implemented into the TSR (Testspeicherring) at the MPIK in order to perform ion-impact collisions. This world-wide unique combination has manifold advantages over conventional Remis. The use of a lithium MOT for providing the target atoms offers two benefits: First, the low temperature that can be achieved with a MOT improves the experimental momentum resolution by a factor up to 10. Second, lithium can be used as a target. With its single valence electron, lithium has a hydrogen-like structure and the correlation of the electrons is significantly reduced for L-shell ionization. Hence, these experimental advancements will help to disentangle effects due to experimental resolution, electronic correlation, and multiple scattering processes in the collision dynamics.

Experimentally, the combination of laser cooling and COLTRIMS is quite challenging. The incompatibility of the Remi's homogeneous magnetic field and the MOT's quadrupole field make it very difficult to measure the electrons' momenta, since the electrons' motion is very sensitive to inhomogenities of the magnetic field. Thus, usually only the recoil ions' momenta are determined with so called MOTRIMS which are a combination of an ion spectrometer and a MOT [BFC+08], [vdPNGA01], [THK+01]. The attempts to also measure the electrons' momenta

have not been successful yet [Ste07].

This diploma thesis deals with the development of a source of slow lithium atoms that is used for loading the target MOT of the MOTRemi. The source has to fulfil special demands that arise from the combination of MOT and Remi and the implementation into the TSR: The vacuum in the reaction chamber which is connected to the TSR needs to be at least at the scale of 10^{-10}mbar in order to ensure a long life time of the stored ion beam in the TSR. Further, the used source must not produce magnetic stray fields within the reaction chamber in order to avoid an influence on the electron trajectories in the spectrometer. For this reason, the distance between the source and the MOT is comparably large and about 40 cm. Nevertheless, a high flux of cold atoms through the capture region of the MOT needs to be obtained in order to achieve shortest loading times.

These requirements are best met by a two-dimensional magneto-optical trap (2D-MOT) [TGLW09]. This 2D-MOT has several advantages of over other possible methods. The hot lithium atoms emerge from an oven perpendicular to the loading direction. They are transversally cooled and then steered towards the MOT by a 'push' laser. Thus, no fast atoms are in the atom beam and the vacuum within the reaction chamber is almost unaffected by the source. The atomic flux that was achieved by Tiecke et al. [TGLW09] is about $10^9/s$. The transversal cooling of the atoms effects a collimation of the atom beam which increases the fraction of the beam that passes through the capture region of the MOT. Therefore, a high loading rate can be accomplished. The magnetic field of the 2D-MOT is mainly perpendicular to direction towards the MOT and due to the collimation the 2D-MOT can be positioned at a distance so that the magnetic field does not disturb the electron spectrometer. In the scope of this thesis a 2D-MOT based on the design by Tiecke et al. [TGLW09] was adapted and optimized to our requirements and a first experiment was perfomed to test the properties of this 2D-MOT.

2 Laser Cooling and Trapping

2.1 Laser Cooling

At present, laser cooling is an often applied method for cooling neutral atoms and ions in order to provide them as cold targets for high resolution spectroscopy or the study of exotic ultra-cold states such as the Bose-Einstein condensate. The principles of laser cooling can be explained best on a simple two-level atom with a ground state $|g\rangle$ and an excited state $|e\rangle$.

2.1.1 Spontaneous Force

When an atom absorbs a photon, not only the energy has to be conserved, but also the total momentum. The momentum of the photon $p = \hbar k$ is transferred to the atom. The excited atom spontaneously emits a photon, dependent on the life time of the excited state, and the momentum transfer of this process has the same absolute value but a random direction. In a laser field all incoming photons have the same momentum $\mathbf{p}$ and the momentum transfer per absorption is $\Delta p = \hbar k$, whereas the spontaneous emission is isotropic and the average momentum transfer after many emissions is zero.

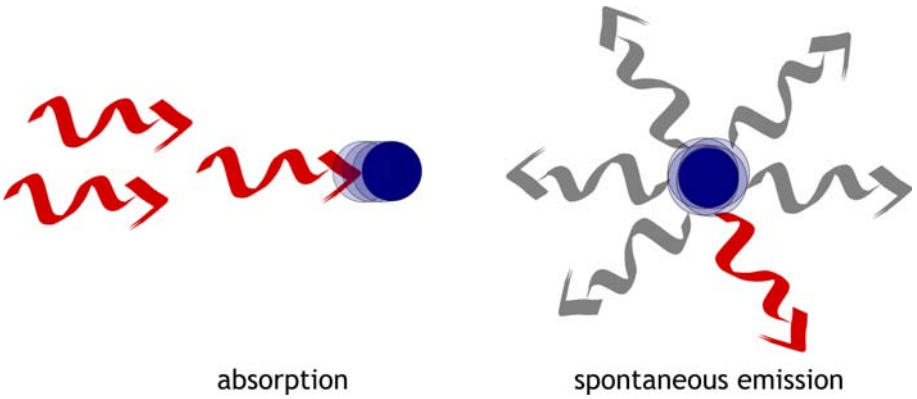

Figure 2.1: Spontaneous Force

This results in a force

$$F = \hbar k \gamma \tag{2.1}$$

an atom experiences in a laser field. γ is the scattering rate, which is the product of the natural width Γ of the excited state and of the fraction of the population of the excited state ρ_{ee}.

$$\gamma = \Gamma \rho_{ee} \tag{2.2}$$

The population ρ_{ee} can be derived from the solution of the optical Bloch equations [MvdS99]:

$$\rho_{ee} = \frac{\frac{s_0}{2}}{1 + s_0 + (2\delta_0/\Gamma)^2} \tag{2.3}$$

with the detuning of the laser δ_0, the difference of the resonance frequency ω_0 and the laser frequency ω_l

$$\delta_0 = \omega_0 - \omega_l, \tag{2.4}$$

and the saturation parameter s_0

$$s_0 = \frac{I}{I_s} \tag{2.5}$$

where

$$I_s = \frac{\pi h c 2\pi \Gamma}{3\lambda^3} \tag{2.6}$$

is defined as saturation intensity at which 25 % of the atoms are in the excited state.

The spontaneous force on an atom at rest is dependent on the laser intensity I and on the detuning δ_0. It has a maximum for $\delta_0 = 0$ and saturates for high laser intensities to F_{max}:

$$I \to \infty : F_{max} = \hbar k \frac{\Gamma}{2} \tag{2.7}$$

As shown in Fig. 2.2 the maximum broadens with higher saturation parameters s_0.

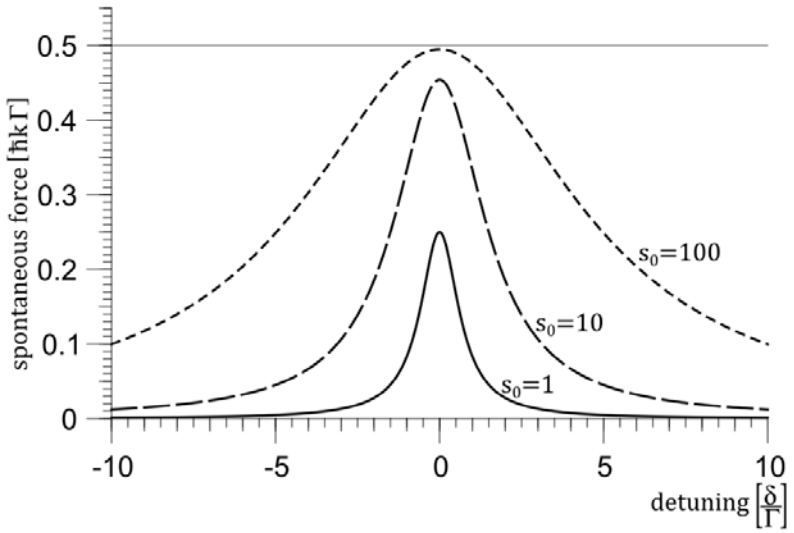

Figure 2.2: Spontaneous force for different saturation parameters

2.1.2 Doppler Cooling

Regarding the motion of an atom the Doppler effect has to be taken into account. Due to this, the frequency ω_l is shifted for an atom with a velocity $\mathbf{v}$ with respect to the rest frame of the light source. In the rest frame of the atom, the Doppler shift of the laser light is $\delta_{Dop} =$ **kv**. Thus, the total detuning δ is

$$\delta = \omega_l \quad \omega_0 \quad \mathbf{kv}. \tag{2.8}$$

The force on the atom is now velocity dependent:

$$F = \hbar k \quad \frac{\frac{s_0}{2}}{1 + s_0 + (2(\omega_l \quad \omega_0 \quad \mathbf{kv})/\ )^2} \tag{2.9}$$

The spontaneous force is maximal when the Doppler shift compensates the detuning of the laser δ_0 and the total detuning δ is zero. The Doppler shift is positive for an opposing laser beam. Thus a red-detuned laser beam, which has a lower frequency with respect to the resonance frequency, gets closer to resonance.

2.1.3 Optical Molasses

In a one-dimensional model, an atom in the field of two counter-propagating laser beams, which are both red-detuned, with wave vectors $\mathbf{k}$ and $-\mathbf{k}$ is closer to resonance with the oncoming beam. The beam with the wave vector parallel to the velocity becomes even more red-detuned and off resonance. Therefore the spontaneous force decelerates the atom. The total spontaneous force of the laser field is the sum of the forces induced by one laser:

$$F^{\mp} = \hbar k \Gamma \frac{\frac{s_0}{2}}{1 + s_0 + (2(\omega_l - \omega_0 \pm \mathbf{kv})/\Gamma)^2} \tag{2.10}$$

$$F = F^{-} + F^{+} \tag{2.11}$$

For $|kv| \ll \Gamma$ the total force F can be approximated by following the linear expression

$$F = \hbar k^2 \frac{8 s_0 \delta/\Gamma}{(1 + s_0 + 4(\delta/\Gamma)^2)^2} \cdot v = -\beta \cdot v, \qquad \beta \geq 0 \tag{2.12}$$

This corresponds to a viscous damping of the motion of the atom. To extend this setup to three dimensions, three orthogonal pairs of counter-propagating laser beams create a light field in which an atom moves as if it was in a viscous liquid, hence this configuration is called an 'optical molasses'.
The trapped atoms cannot be cooled down to absolute zero, since this is forbidden by thermodynamics. Therefore the question arises what the cooling limit is. The temperature which can be achieved with this method has an upper limit called the Doppler cooling limit which is caused by heating effects due to the random nature of the spontaneous force and the finite momentum transfer of $\hbar k$ of every absorption and emission, see [MvdS99]:

$$T_D = \frac{\hbar \Gamma}{2 k_B} \tag{2.13}$$

2.1.4 Cooling of ^{7}Li

In the discussed two-level atom model, the spontaneous force is a result of a cycle of the absorption and subsequent emission of a photon, a cycle between ground state

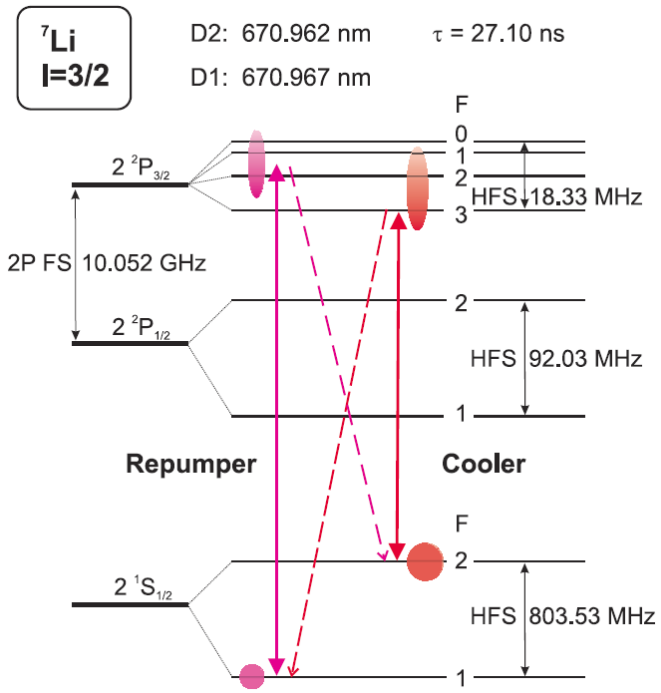

Figure 2.3: Schematic drawing of the ^{7}Li atomic levels used for laser cooling: The continuous arrows depict the transitions driven by the cooling and the repumping lasers, the dashed arrows the decay into the ground state that is dark for the prior transition. F: Fine structure splitting, HFS: hyperfine splitting, τ: lifetime of the excited state [Ste07].

and excited state. This *closed* or *cycling transition* is granted in a two level system. But with lithium it is not so trivial. ^{7}Li is a multi-level atom, which makes the laser cooling more complex. More than one transition exists and it is possible that an excited state is able to decay into another than the initial ground state, which then cannot be excited again by the cooling laser, a so called dark state. By using such an open transition, the atoms are optically pumped from the original ground state to the dark state and cannot be cooled further without additional effort.
A completely closed transition does not exist for ^{7}Li. Thus a second laser with a different frequency has to be applied, which repumps the atoms to the original ground state. In Fig. 2.3 the cooling cycle, which is used for cooling ^{7}Li, is shown. The cooling transition $|2^2S_{1/2}\rangle$ to $|2^2P_{3/2}\rangle$ is the D2-component of the D-line. The transition from $|2^2S_{1/2}, F = 2\rangle$ to $|2^2P_{3/2}, F = 3\rangle$, which is driven by the cooling laser, is in principle closed since the selection rules for dipole transitions forbid other decays. However whereas the hyperfine splitting of the ground state is 803.53 MHz, which is large enough to seperate them for the laser, the hyperfine splitting of the $|2^2P_{3/2}\rangle$ state is over all total angular momenta just 18.33 MHz, which corresponds to three natural linewidths and makes an off-resonance transition into those states possible, see Fig. 2.2. Thus hyperfine states with another total angular momentum can be excited. The states $|2^2P_{3/2}\rangle$ with a total angular momentum $F \ll 3$ can also decay into the ground state with $F = 1$. The repumping laser drives the transition from $|2^2S_{1/2}, F = 1\rangle$ to $|2^2P_{3/2}, F = 2\rangle$ Therefore this three level circle is closed.

2.2 Magneto-Optical Trap

The optical molasses only confines atoms in the momentum space. In order to spatially confine the cooled atoms, a position dependence of the detuning and thus a position dependence of the force is needed. In a magneto-optical trap (MOT) this is done by using the Zeeman shift induced by an inhomogeneous magnetic field.

2.2.1 Working Principle of a MOT

The basic working principle of a MOT can be well explained with a simple one-dimensional model. The model atom is a two-level atom with a ground state $|g\rangle$ with a total angular momentum $F = 0$ and with an excited state $|e\rangle$ with a total angular momentum $F = 1$. The magnetic field of the MOT is a gradient field along the z-axis

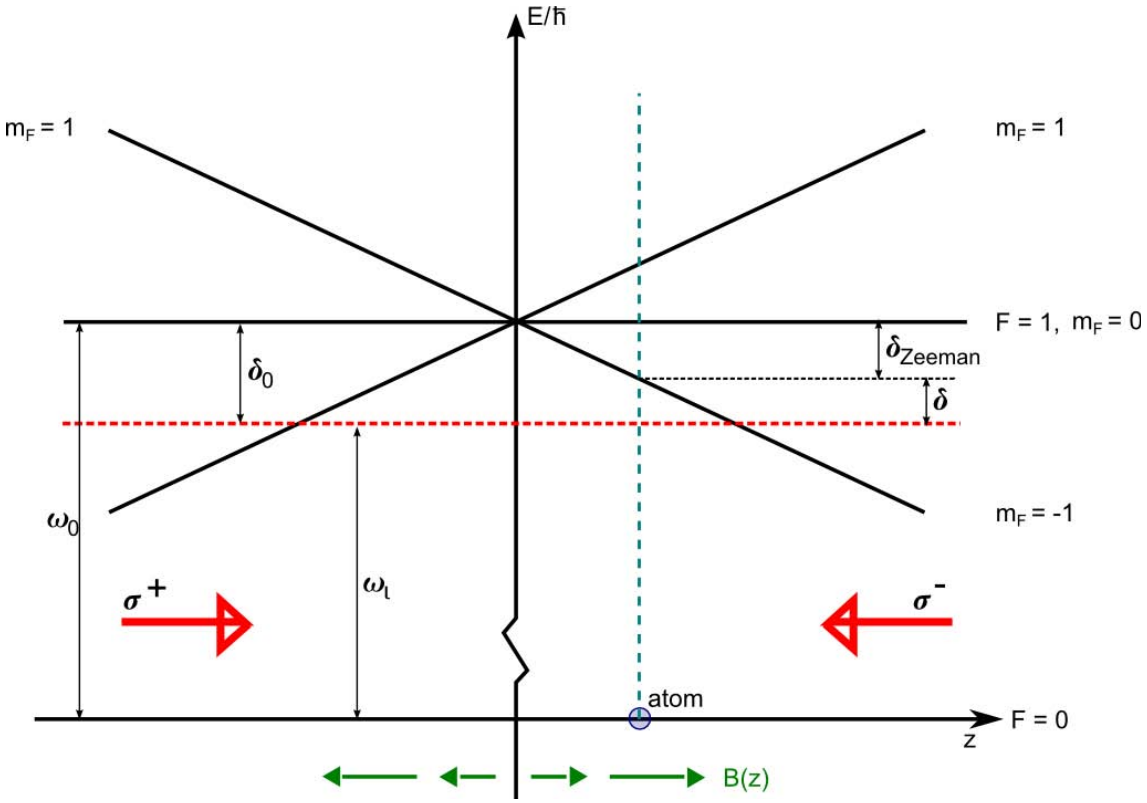

Figure 2.4: One-dimensinal model of a MOT: A transition from a state with a total angular momentum $F = 0$ to a state with $F = 1$ is induced. A magnetic field gradient causes the Zeeman splitting. The energy levels of the atom are depicted by the continuous black lines. The red dashed line depicts the energy of a photon of the laser. The laser beams are depicted by the red arrows. The circular polarization is labeled with respect to the atom's quantisation axis, e.i. the direction of the magnetic field.

$B(z) = \frac{\partial B(z)}{\partial z} \cdot z = B'_z z$. The atom is illuminated by a pair of counter-propagating, red-detuned circular polarized laser beams with opposite circular polarisations. The magnetic field breaks the degeneracy of the excited state due to the Zeeman effect. The Zeeman shift of energy is

$$\Delta E = \mu_B g_F m_F B = \mu m_F B \tag{2.14}$$

with the Landé g-factor g_F. So the total detuning is

$$\delta = \delta_0 \quad \mathbf{kv} \quad \mu m_F B(z)/\hbar. \tag{2.15}$$

In the magnetic field the transition from ground state $|F = 0, m_F = 0\rangle$ to

$|F = 1, m_F = -1\rangle$ is closer to resonance with the red-detuned laser, whereas the transition to $|F = 1, m_F = 1\rangle$ is more off resonance. Due to selection rules for dipole transitions, changes of the magnetic quantum number $\Delta m_F = \pm 1$ are only possible with circular polarized light σ^+/σ^-, where σ^+ is defined as light that drives transitions with $\Delta m = +1$. The transition with $\Delta m_F = 0$ needs linear polarized π-light. Since the laser light is circular polarized, the transition from $|F = 0, m_F = 0\rangle$ to $|F = 1, m_F = 0\rangle$ is forbidden. Thus mainly σ^--light is scattered with the atom. If the circular polarisation is chosen appropriately, the spontaneous force pushes the atom towards the center. An atom at a position $z > 0$, as shown in Fig. 2.4, preferentially scatters with σ^--light coming from the right and thus the atom is driven back to the center. When the atom crosses zero, the magnetic field changes direction and thus the quantization axis of the atom flips. The light coming from the left now is seen as σ^--light by the atom and the atom is pushed to the center again. The force on an atom, which is induced by one laser beam is

$$F^{\mp} = \hbar k \Gamma \frac{\frac{s_0}{2}}{1 + s_0 + (2(\omega_l - \omega_0 \pm \mathbf{kv} + \mu_B g_F \Delta m_F B(z)/\hbar)/\Gamma)^2} \tag{2.16}$$

The total force is the sum:

$$F = F^+ + F^- \tag{2.17}$$

The total force can be linear approximated similar to the approximation (2.12) of equation (2.11) under the condition $|kv| \ll \Gamma$:

$$F = \hbar k^2 \frac{8 s_0 \delta/\Gamma}{(1 + s_0 + 4(\delta/\Gamma)^2)^2} \cdot v + \hbar k \frac{\mu_B g_F \Delta m_F B'_z}{\hbar} \frac{8 s_0 \delta/\Gamma}{(1 + s_0 + 4(\delta/\Gamma)^2)^2} \cdot z \tag{2.18}$$

$$F = -\beta \cdot v - D \cdot z, \quad D \,\text{and}\, \beta > 0 \tag{2.19}$$

This is the equation of motion of a damped oscillator with the spring constant D and the damping constant β. In a MOT, the atom's motion is usually overdamped.

2.2.2 Basic Setup of a MOT

The basic setup of a MOT is shown in Fig. 2.5. A magnetic quadrupole field is created by a pair of anti-Helmholtz coils, i.e. two coaxial coils with opposite current.

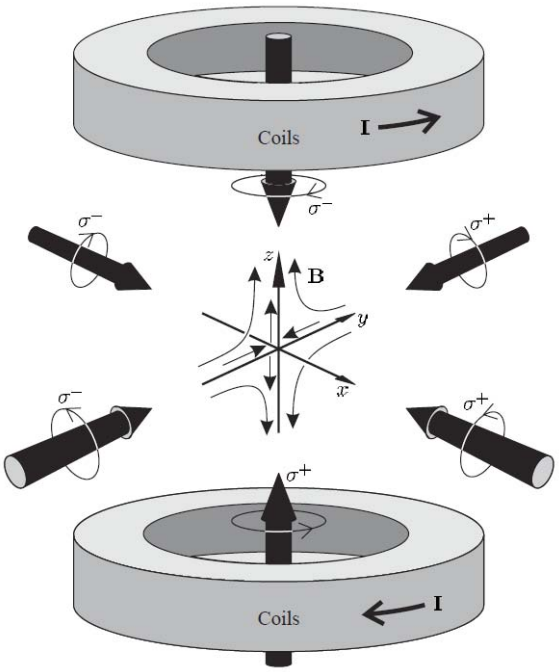

Figure 2.5: Scheme of a MOT setup: Two coils with opposite current **I** create a magnetic quadrupole field. The field is denoted by field lines in the y-z-plane. The cooling laser beams are shown as arrows with circular arrows denoting their circular polarization. Figure by Foot [Foo05]

Due to the symmetry of the coils the magnetic field is cylindrically symmetrical. The quadrupole field has a strong gradient in the radial and axial directions in a region around the trap center, which is positioned on the symmetry axis at half the distance between the coils. The magnetic field strength is zero in the center, where three orthogonal pairs of counter-propagating laser beams intersect. The beams have a diameter of a few cm and have the appropriate circular polarization. Although the magnetic field is cylindrically symmetrical, it is feasible to choose a Cartesian coordinate system with the axes parallel to the laser beams and the origin in the trap center to describe the MOT, since the single spontaneous forces act in the beam directions.

2.2.3 Properties

Having described the working principles of a MOT, some properties of it remain to be discussed which determine its usefulness. The distance R_c, where the Zeeman shift compensates the detunig of the laser δ_0, is the *capture radius* of the MOT.

$$R_c = \frac{\hbar\delta_0}{\mu B'} \tag{2.20}$$

Beyond the capture radius the atom cannot come in resonance with the opposing laser and will not be forced back to the center if it has a velocity $v \geq 0$ in the direction away from the center.
The maximum velocity which an atom can have in order to still be captured is called the *capture velocity* v_c. It can be estimated by the assumption that the decelaration of an incoming atom basically works like a Zeeman slower (see section 2.3.1).

The upper limit for the capture velocity v_c is the velocity at which the Doppler shift compensates the Zeeman shift, which is induced by the maximum of the magnetic field.

$$|v_c| \leq \frac{\mu m_F B_{max}}{\hbar k} \tag{2.21}$$

This assumes that the spontaneous force is maximal over the distance from the position with maximal field strength to the stopping position. Of course this is not the case, if the laser intensity is too low at any position along the slowing distance. Furthermore, for high field strengths the working principle of a Zeeman slower cannot be used anymore to describe the capturing, since the gradient of the magnetic field

is to strong to slow down high velocities, see eqution (2.23). The capture velocities are at the scale of a few $10\frac{m}{s}$.
Since Doppler cooling is used in a MOT, it seems obvious that the achievable temperatures of the trapped atoms can be as low as the Doppler limit T_D (see equqtion (2.13)). However, the temperature can be even lower, which has already been discovered in the first implementations of magneto-optical traps. This is due to effects induced by the spatially varying polarization vector of the light field, which is caused by the superposition of the cooling beams [MvdS99].

2.3 Loading a Magneto-Optical Trap

An efficient loading of the MOT is crucial to optimize the duty cycle in the short beam times available. The atoms come from a source with a high temperature. In the case of lithium, the oven is operated at a temperature of 350°C in order to assure a sufficient atomic flux. Maxwell-Boltzmann-distribution of velocities at this temperature leads to an mean velocity of about 1400 m/s. However, a MOT can only capture atoms with a velocity up to the capture velocity v_c, which is in the range of several 10 m/s. Thus, in order to ensure a high loading rate of the MOT, the atoms have to be pre-cooled.
The simplest way of loading a MOT is the capture from vapor. A despenser creates a cloud of atoms which surrounds the MOT. The atoms with a sufficiently low velocity within the capture region are cooled and confined, a so called vapor-cell MOT. The major drawback of this method is the high background pressure. Thus, the life time of the trapped atoms is limited by collisions with faster atoms from the vapor and the pressure causes high backgrounds in experiments or makes experiments even impossible. For lithium, additional problems occure: The vapor pressure is negligible for temperatures with which a conventional vacuum system can be operated, i.e. the baking temperature. Further, lithium is chemically reactive with glass and therefore a vapor cell is not compatible with optical cooling. Thus, loading methods with atomic beams have to be used. In the following methods that have been considered for this project are discussed with which the highest optically cooled atom fluxes to date have been achieved [TGLW09], [SK05], [SVH05]. have been produced.

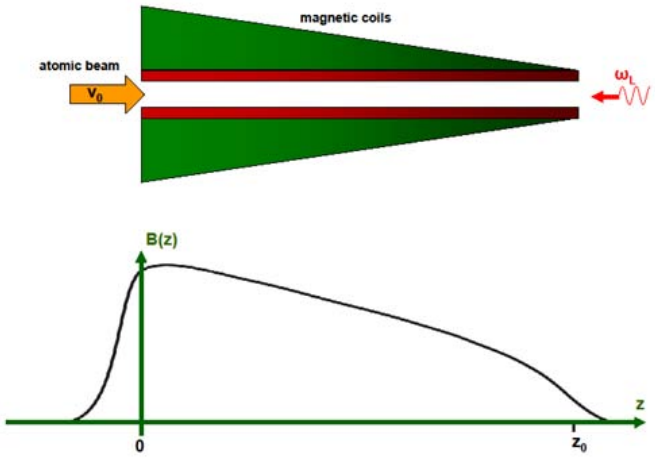

Figure 2.6: Working principle of a Zeeman slower: The hot atoms are opposed by a red-detuned laser. The magnetic field B(z), here created by coils with decreasing number of windings, develops as depicted in the graph.

2.3.1 Zeeman Slower

The Zeeman slower is a commonly used method to decelerate atoms from thermal velocities up to $v \approx 1000\,m/s$ (the average speed of Li at 350°C is 1400 m/s) to only a few m/s. The fast atoms emerge from their source through a tube along the z-axis, thus their velocities are mainly in z-direction. A counter-propagating, slightly red-detuned laser beam illuminates the atoms. Since the velocities are Maxwell-Boltzmann-distributed, atoms with a wide range of velocities have to be slowed down. Therefore, a specific magnetic field is added, which decreases with the distance to the hot atom's source. This induces a distance dependent Zeeman shift which compensates the Doppler shift of one defined velocity at each position $kv = \delta_{Zeeman}$. The magnetic field has to decrease in a way so that an atom, which once is in resonance and therefore decelerated, stays in resonance. If the magnetic field strength drops too strongly, the maximal deceleration is not sufficient to change the velocity fast enough and the atom falls out of resonance.
The maximal decelaration of an atom is, according to equation (2.7), $a_{max} = \hbar k \frac{}{2m}$ with the atom's mass m. Usually one calculates the magnetic field for a deceleration $a = \eta a_{max}$ with $0 < \eta < 1$ to ensure that an atom cannot slip out of the cooling cycle due to fluctuations in the magnetic field or in the laser intensity. The longitudinal

velocity in dependence of the position is

$$v(z)^2 = v_{max}^2 - 2a \cdot z. \tag{2.22}$$

v_{max} is the maximum velocity that can be slowed down by the Zeeman slower, determined by the maximum of the magnetic field. With equation (2.22) and equation (2.15) one obtains the spatial dependence of the magnetic field:

$$B(z) = \frac{\hbar}{\mu}(\delta_0 + k\sqrt{v_{max}^2 - 2a \cdot z}) \tag{2.23}$$

The distance which is necessary to stop the atoms is according to equation (2.22):

$$d_{slower} = \frac{v_{max}^2}{2a} = \frac{v_{max}^2}{2\eta a_{max}} \tag{2.24}$$

The disadvantage of a Zeeman slower is that the atoms are only cooled in the longitudinal direction and even heated up in the transverse plain. The slow atom beam diverges significantly. Thus, the fraction of atoms which reach the trapping region decreases with increasing distance from the Zeeman slower. Atoms which are too fast, so that the Zeeman shift at the position of maximum magnetic field cannot compensate the Doppler shift, are not decelerated and are not filtered out. Thus, there is always a fraction of fast atoms in the beam.

2.3.2 2D-MOT

Basically, a two-dimensional MOT (2D-MOT) works like a regular MOT. However, in a 2D-MOT as a source for a cold atom beam, the atoms are only cooled transversally to the z-axis, which lies in the direction of the MOT that is loaded. Thus it only uses two perpendicular pairs of counter-propagating laser beams with circular polarized light (as described for a MOT) along the x- and y-axes. The magnetic field is a two-dimensional quadrupole field with a strong field gradient in the x- and y-directions and zero field strength along the z-axis. The hot atoms enter the 2D-MOT almost perpendicular to the z-axis. They are cooled in the x- and y-components v_x and v_y of their velocities, while v_z is not cooled. After the cooling the atoms have a velocity $\mathbf{v} = v_z\mathbf{e}_z + \delta\mathbf{v}$ which is almost equal to the initial velocity in the z-direction. $\delta\mathbf{v}$ consists of the remaining transversal velocity and of the veloc-

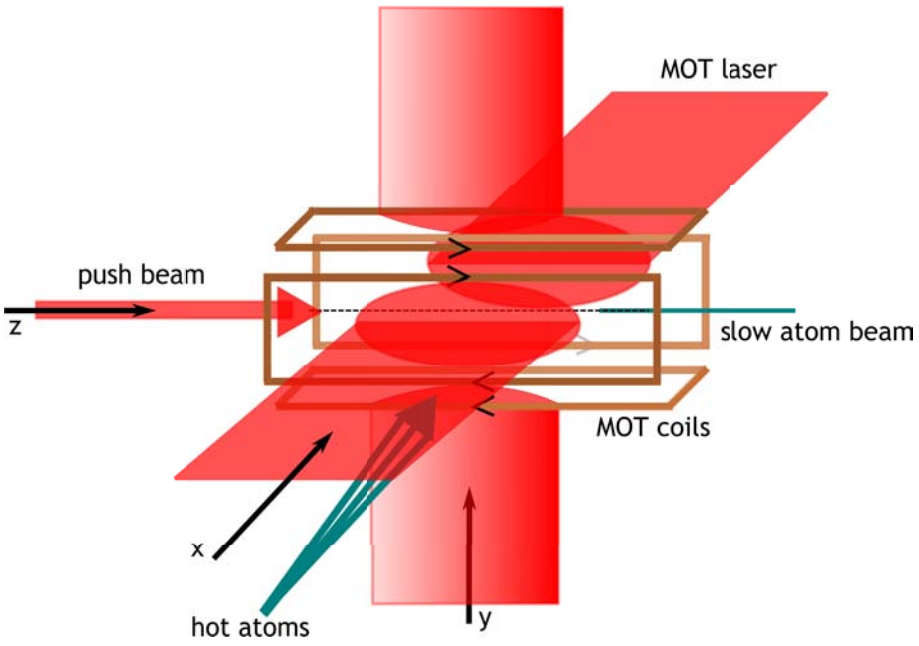

Figure 2.7: Working principle of a 2D-MOT: Hot atoms enter the cooling region in a 45° angle in the x-y-plane. The transversally cooled atoms move along the z-axis and emerge in a beam of slow atoms from the 2D-MOT directed by the pushing laser beam.

ity change in z-direction due to the heating. The atoms are trapped in a cylindrical volume around the z-axis and would move out at either side in positive or negative z-direction. In order to push all slowed atoms towards the recapturing MOT, a single slightly red-detuned 'push' laser beam along the z-axis illuminates the center of the 2D-MOT inducing a spontaneous force in the direction of the MOT. For the pushing, no repumper (see section 2.1.4') is used, thus the atoms eventually fall into the dark state and the acceleration of the atoms is limited in order to provide a slow beam. The maximum of v_z is determined by the geometry of the experimental setup. Two apertures, or alternatively a tube, connecting the hot atom source with the 2D-MOT, limit v_z in dependence of the of the other velocity components. The maximum velocity in z-direction of an atom emerging from the second aperture is

$$v_z < \frac{d}{l} v_{x'} \tag{2.25}$$

with the apertures' opening radius d and the distance l between them.
The maximum velocity of atoms which leave the 2D-MOT after the cooling in the slow atom beam is dependent on the maximum capture velocity v_c (see eqution

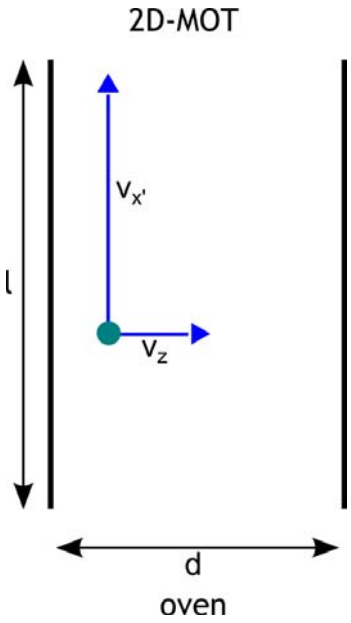

Figure 2.8: Atom moving through a tube that is connecting the oven with the 2D-MOT. The geometry of the tube limits the maximal velocity in z-direction v_z in dependence of the velocity longitudinal to the tube $v_{x'}$. l: Length of the tube, d: diameter

(2.21)) of the 2D-MOT:

$$v_{z,final} < \frac{d}{l} v_c \tag{2.26}$$

The beam of cold atoms from the 2D-MOT is well collimated. Thus a large fraction of the cooled atoms can be recaptured in the MOT. No atoms with a velocity greater than the capture velocity of the MOT, which could spoil the vacuum or collide with already trapped atoms and thrust them out of the trap, are present in the beam.

3 Reaction Microscope

The Reaction Microscope (Remi) - often refered to as COLTRIMS (Cold Target Recoil Ion Momentum Spectrometer) was developed by Ullrich et al. [UMD+97] and allows to perform kinematically complete experiments on particle impact ionization. The momentum vectors of the recoil ion and of the emitted electrons are measured over a solid angle of almost 4π. With a statistically sufficient number of measured events it allows to determine fully differential cross-sections (FDCS). The Remi has become standard device that is used in facilities all over the world. In the MPIK allone, 10 Remis are in operation.

3.1 Working Principle of a Remi

To measure the momentum of the recoil ion in a COLTRIM spectrometer the ion is extracted by a weak homogeneous electric field (usually a few V/cm) towards a detector, which is two-dimensionally position sensitive in a plane perpendicular to the electric field.Knowing the time of flight and the position on the detector, it is possible to derive the momentum of the detected ion.

The emitted electrons are also extracted by the electric field to the opposite side, where another two-dimensional position sensitive detector is located. This one is capable of detecting multiple hits within a time of a few 10 ns, which is important to investigate multi ionization processes. Due to their small mass, the emitted electrons, which have momenta of about same magnitude as the recoil ions, are significantly faster than the ions. Thus they cannot be guided alone by the electric field towards the detector, which covers only a small solid angle. Hence a homogeneous magnetic field with a field strength of a few Gauss parallel to the electric field is applied. The Lorentz force leads the electrons on spiraling trajectories. Therefore also electrons with a large transverse kinetic energy, in contrast to the energy which they gain in the extraction field,can be projected on the detector. Since the Lorentz

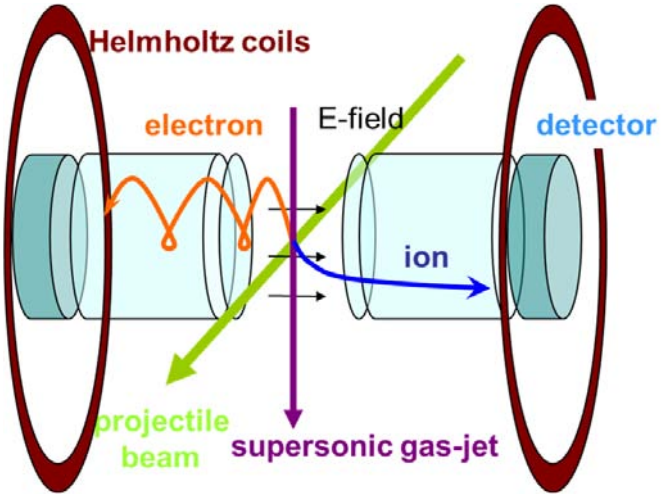

Figure 3.1: Schematic diagram of a reaction microscope

force is orthogonal to the magnetic field, the longitudinal motion is not affected. An upper limit for the transverse momentum that can be measured is set by the size of the detector and the strength of the magnetic field, the radius of the cyclotron trajectoreis is $r_e = \frac{p_\perp}{eB}$ with the transversal momentum $p_\perp$. For example, an electron with a transverse kinetic energy of 100 eV is forced on spiral with a radius $r_e = 3.4\,cm$ in a magnetic field of 100 gauss. The active region of the detector must have at least double this radius to detect the electron, see Fig. 3.2 The magnetic field does not considerably affect the recoil ions' trajectories due to their high mass.

A sketch of a typical Remi is shown in Fig. 3.1. The electric field is located around the reaction region. The homogeneous magnetic field is parallel to the direction of extraction and is generate by a pair of Helmholtz coils. The projectile beam hits the target in the reaction volume. Optionally, electric field-free drift regions are adjacent on the field on either side in the direction of extraction. The proportion of the lengths of drift and aceleration regions can have several effects, such as time or position focusing. If the lengths of the drift regions (d_e, d_i) is double the length, in which the electrons or the ion, respectively, are accelerated (a_e, a_i), this proportion leads to a time focusing [Fis03], i.e. the time of flight of particles, which are initially at rest, is inured to small variations of the starting position. Thus the extent of the reaction volume does not affect the time of flight, if the volume is small enough. The drift regions end at the two-dimensional position sensitive detectors.

3.1.1 Deriving the Momenta

Since the motion, which is longitudinal to the direction is only dependet on the time of flight and the transversal motion is dependent on position and time of flight, it is intuitive and useful to split the momenta into a component perpendicular and a component parallel to the direction of extraction: $\mathbf{p} = \mathbf{p}_\perp + \mathbf{p}_\parallel$. Regarding the symmetry of the Remi, it is reasonable to use cylindrical coordinates, with $p_\parallel$ in axial direction and $p_\perp$ in radial direction under an angle φ in the plane perpendicular to the symmetry axis.

The Longitudinal Momentum

It is possible to calculate the longitudinal momentum component $p_\parallel$ with the particle's time of flight [Fischer]. After the ionization and the resulting momentum transfer in the collision, the particle is accelerated over the distance a by the electric field. After that it flies over the distance d through the drift region to the detector. The time of flight of the recoil ion or the electron, respectively, is

$$t_\pm(E_\parallel) = f \cdot \sqrt{m} \left(\frac{2a}{\sqrt{E_\parallel + qU} \pm \sqrt{E_\parallel}} + \frac{d}{\sqrt{E_\parallel + qU}} \right) \tag{3.1}$$

with $f = 719.9 \cdot \frac{ns}{cm} \sqrt{\frac{eV}{amu}}$, a and d in cm, $E_\parallel$ and qU in eV and the mass m in atomic units amu. The '+' sign has to be used for the case of initial momentum towards the detector, '-' in the other case of initial momentum in the opposite direction.
The inverse function of equation (3.1) has to be determined to obtain the longitudinal momentum. This is only possible with approximations or numerical approaches. Further, the time of flight can only be measured related to a trigger signal by the projectile beam.
Since the kinetic energy $E_{r\parallel}$ of the recoil ion amounts to a few meV and is therefore small compared to the energy qU, which the ion receives in the accelerating electric field and which is a few eV, one can approximate the difference Δt_r between the time of flight of an ion with initial longitudinal kinetic energy $E_{r\parallel} = 0$ and of an ion with energy $E_{r\parallel} \neq 0$:

$$\Delta t_r = t(E_{r\parallel}) - t(E_{r\parallel} = 0) \approx \left[\frac{dt_r(E_{r\parallel})}{dE_{r\parallel}} \cdot \frac{dE_{r\parallel}}{p_{r\parallel}} \right]_{p_{r\parallel}} \cdot p_{r\parallel}. \tag{3.2}$$

Equations (3.2) and (3.1) together lead to the following expression for the recoil ion:

$$p_{r\parallel} = \left(8.04 \cdot 10^{-3} \frac{cm \cdot a.u.}{eV \cdot ns}\right) \frac{qU}{a} \Delta t_r \tag{3.3}$$

The electrons' initial kinetic energy is in the same order of magnitude as the energy gained in the electric field. Thus the determination of the inverse function is more difficult. Both analytical and numerical approximations are used in Remi experiments. Discussing this goes beyond the scope of this work, please be referred to Fischer [Fis03].

Recoil Ion

Neglecting the small kinetic energy of the recoil ion $E_{r\parallel}$ one obtains with equation (3.1):

$$t_r(E_{r\parallel} = 0) = f \cdot \sqrt{\frac{m}{q}} \cdot \frac{2a + d}{\sqrt{U}}. \tag{3.4}$$

The time of flight is dependent on the ratio of mass and charge. Thus it is possible to distinguish the ionization processes, e.g. between single and double ionization, by analyzing the peaks in the time of flight spectrum of the recoil ion. The difference of the time of flight for different charge states is a few μs, whereas the difference caused by the recoil momentum is only a few ns. Thus, each charge state can be identified by clearly seperated peaks.

The Transversal Momentum

The transversal momenta can be derived from the position where the particle hits the detector and the time of flight. The position on the detector is given in polar coordinates, the determination of the origin is dependant on the symmetry of the spectrum which is dependant on the particular experiment, see Fig. 3.2
The recoil ion's transversal momentum can be calculated easily. The transversal motion is not affected by the electric extraction field. And the effect of the magnetic field can also be neglected due to the ion's mass. Thus, the ion's transversal velocity is constant in time. After the time of flight t_r it has traveled a transversal distance

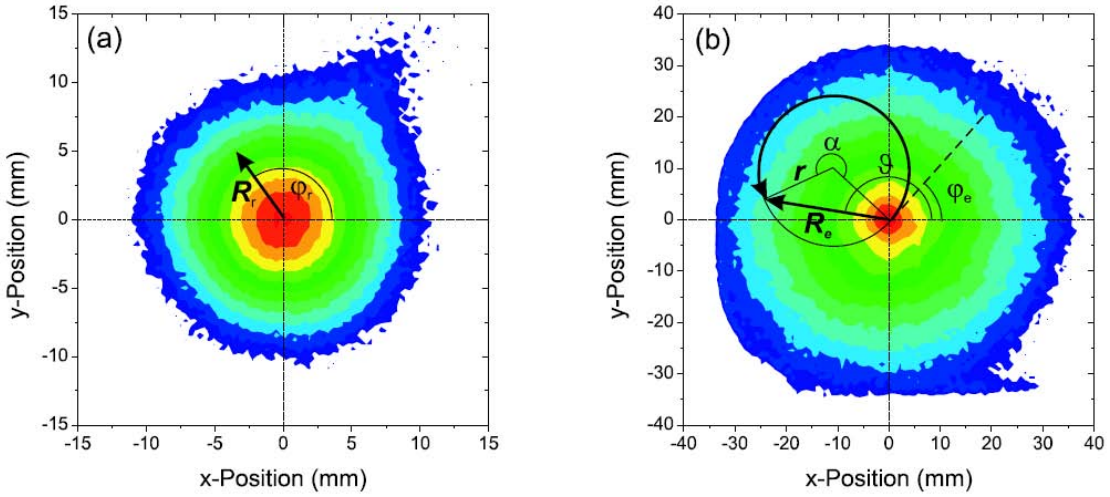

Figure 3.2: Example for position spectra [Fis03]: (a) for recoil ions, (b) for electrons. The depicted parameters are necessary for the calculation of the particels' momenta. Since these spectra have a symmetry point, this point was chosen for the origin.

R_r and hits the detector at (Fig. 3.2):

$$R_r = \left(1.2 \cdot 10^{\ 3} \frac{mm \cdot amu}{ns \cdot a.u.}\right) \frac{p_\perp \cdot t_r}{m_r} \tag{3.5}$$

under the angle φ, which is the angle defining the direction of $p_{r\perp}$. The approximated time of flight, see equation (3.4), can be used for the calculation of $p_{r\perp}$. Thus the transversal momentum of the recoil ion is in atomic units:

$$p_{r\perp} = \left(11.6 \cdot \frac{a.u.}{\sqrt{amu \cdot eV}}\right) \frac{R_r}{2a+d} \sqrt{qUm} \tag{3.6}$$

An electron follows cyclotorn trajectories in the transversal plane with radius r

$$r = \frac{p_{e\perp}}{eB} \tag{3.7}$$

and cyclotron frequency

$$\omega_c = \frac{eB}{m_e}. \tag{3.8}$$

For the time of flight t_e the electron moves along the circle over an angle $\alpha = \omega_c t_e$. It hits the detector at a position with the distance R_e to the symmetry point.

Geometric calculations (Fig. 3.2) lead to

$$r = \frac{R_e}{2\left|\sin(\alpha/2)\right|} = \frac{R_e}{2\left|\sin(\frac{1}{2}\omega_c t_e)\right|}. \tag{3.9}$$

The equations (3.7) and (3.9) allow to derive the transversal momentum of the electron:

$$p_{e\perp} = \left(8.04 \cdot 10^{-3} \frac{cm \cdot a.u.}{eV \cdot ns}\right) \frac{R_e B}{2\left|\sin(\frac{1}{2}\omega_c t_e)\right|} \tag{3.10}$$

With the angle ϑ, which can be obtained from the position spectrum (Fig. 3.2) one can derive the angle φ_e:

$$\varphi_e = \vartheta - \frac{\omega_c t_e}{2} \tag{3.11}$$

3.1.2 The Resolution of the Reaction Microscope

The resolution of the ion spectrometer is basically limited by the target temperature and time and position uncertainties. The temperature causes an uncertainty of the target's momentum $\Delta p_{thermal}$. The resolution can be calculated with the Gaussian propagation of uncertainty:

$$\Delta p_{\parallel}^2 = \left[\left(8.04 \cdot 10^{-3} \frac{cm \cdot a.u.}{eV \cdot ns}\right) \frac{qU}{a}\right]^2 \cdot \Delta t^2 + \Delta p_{thermal}^2 \tag{3.12}$$

$$\Delta p_{\perp}^2 = \left[\left(11.6 \cdot \frac{a.u.}{\sqrt{amu \cdot eV}}\right) \frac{\sqrt{qU \cdot m_r}}{2a + d}\right]^2 \cdot \Delta R_r^2 + \Delta p_{thermal}^2 \tag{3.13}$$

The resolution of the electron spectrometer is, in contrast to the ion spectrometer, essentially independent of the target temperature, since the kinetic energy, which the electron gains in the ionization process, is several orders of magnitude higher than the thermal energy. For further details see Fischer [Fis03].

4 The PRIOC Project

The PRIOC (**Pr**ecision studies on **I**on **C**ollisions) project uses three state of the art techniques. A magneto-optical trap and a reaction microscope are combined and they are implemented into an ion storage ring, the Testspeicherring (TSR) at the Max-Planck-Institut für Kernphysik (MPIK). It aims at measuring both electrons and recoil ions from a magneto-optically cooled target with a reaction microscope.

4.1 Combining MOT and Remi

4.1.1 The Advantage of the Combination

The combination of a magneto-optical trap (MOT) and a reaction microscope (Remi) to a MOTRemi offers new possibilities. The resolution of the ion spectrometer of a Remi is temperature dependent (see equations (3.12) and (3.13)), thus optimizing the target temperature improves the ion spectrometer. The usual target in experiments with a Remi is a supersonic gas jet which has a temperature at the scale of several 10 mK. A considerable reduction of the temperature is possible, but only with substantial effort and significantly reduced target density. However, a MOT offers this improvement with a temperature of the trapped atoms of a few 100 μK. Furthermore, a MOT enables the use of lithium as an atomic target, which is not possible with a supersonic gas jet. The hydrogen-like structure of lithium, which has only a single valence electron, makes it the ideal atomic target to test state of the art theories for ion-impact ionization which have not completely taken into account possible effects on the collision dynamics due to correlations between the electrons in the target atom. Though it is even possible to use atomic hydrogen, which would be the ideal target, with a supersonic gas jet, the necessary dissociation of the hydrogen molecules leads to a heating of the gas, which would corrupt the resolution. Thus, a MOT provides a superior target at a lower temperature, increasing the resolution of the ion spectrometer and allowing an easier theoretical approach.

4.1.2 Requirements and Problems

The difficulty of combining MOT and Remi is that the magnetic field of a Remi has to be homogeneous and constant, since the electrons' motion is very sensitive to magnetic fields. But the MOT needs a magnetic quadrupole field, which is inhomogeneous. Thus the two systems cannot be operated at the same time, i.e. the MOT field has to be switched off before the collision experiments are performed. The switching induces Eddy currents in the surrounding metal, such as the vacuum chamber, the holder of the MOT coils or the spectrometer of the Remi. These Eddy currents induce magnetic fields, which have a strong impact on the electrons' trajectories. In Fig. 4.1, electron time of flight spectra are shown for different waiting times after the magnetic field is switched off. These spectra were measured by Schuricke et al. with another MOTRemi [Sch08]. The part labeled '1 s' shows the spectrum which is not affected by residual magnetic fields as a reference. After 2 ms, one can roughly identify the pattern of the reference spectrum. However, after this waiting time, the effect of the Eddy currents is still too strong to obtain useful data. Thus, waiting times of a few ms are necessary until the residual magnetic fields disappear with this setup. During that time, the lasers can still illuminate the captured atoms, creating an optical molasses, which still cools the atoms, but does not keep them spatially confined. Therefore, they diffuse, which diminishes the target density, thereby reducing the numbers of events in one experimental cycle. After 2 ms most of the atoms have already defused out of the reaction region. Further, the long waiting times extend the duty cycle. Thus, Eddy currents have to be minimized in order to keep the necessary waiting period as short as possible.
These problems are the reason why so far only the recoil ions have been measured with the combination of a MOT and a Remi in experiments, while the electrons' momenta could not be measured yet.

4.2 The Vacuum Chamber

A very important component of high precision momentum spectroscopy is the vacuum. Laser cooling and especially trapping need a good vacuum, as well. The lifetime of the trapped atoms in the MOT is considerably shortened by collisions with fast atoms of a surrounding gas. Further, hits of the projectile beam with the background gas cause background events of the measurement. The lifetime of the ion beam in the storage ring also depends on the vacuum conditions. Furthermore,

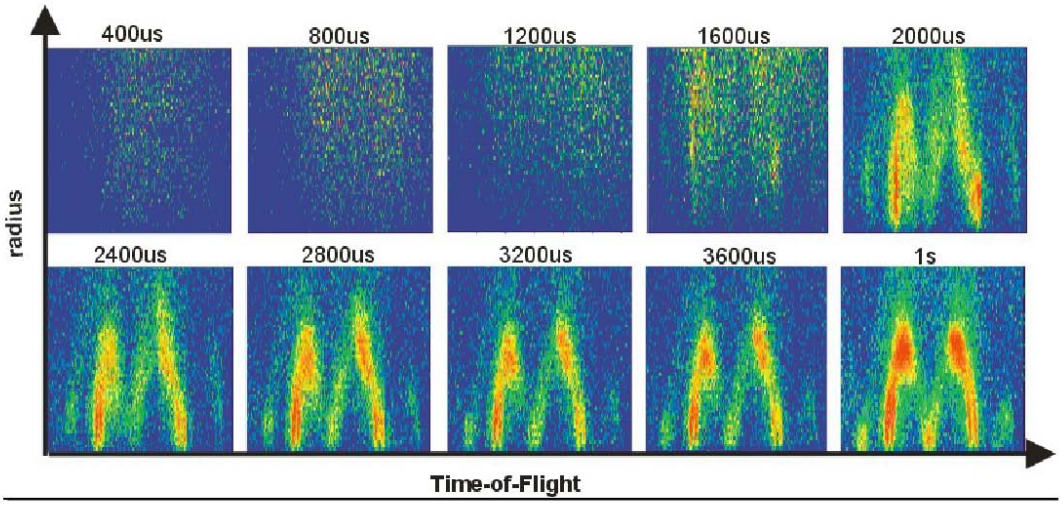

Figure 4.1: Time of flight spectra of electrons for different times after the magnetic MOT field is switched off. The spectrum after 1s shows the spectrum with no magnetic field remaining as reference [Sch08].

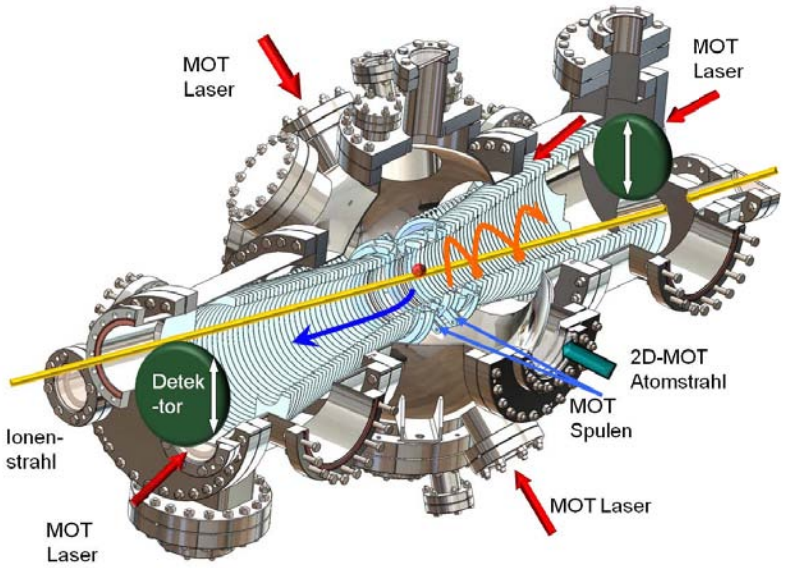

Figure 4.2: The main vacuum chamber with the MOT and the spectrometer

the vacuum chamber has to fulfil the special condition that is given for building a MOTRemi, i.e. no disturbing magnetic fields may be caused by the metal chamber.

The whole vacuum setup consists of the main chamber and the 2D-MOT chamber. They are built with 1.4429 ESU stainless steel with a permeability of less than 1.01 H/m to prevent influences from the chamber on the magnetic field of the electron spectrometer. The inner surface of the chamber is coated with a non evaporable getter material (Neg), which improves the vacuum [egc]. The design of the main chamber is shown in Fig. 4.2. The chamber basically consists of a spherical center with a diameter of 400 mm, which connects two cylindric chambers located at opposite ends of the central part with a diameter of 250 mm. They contain the acceleration and drift tubes of the ion- and electron- spectrometers. The central part mainly contains the MOT, and the diameter of the sphere is chosen in such a way that it provides the sufficient distance to the MOT coils in order to prevent Eddy currents (see section 4.3.1).
The MOT is suspended from the top flange of the main chamber and can be removed through this port. The center part is equipped with four viewports in the central plane perpendicular to the spectrometer's symmetry axis for four of the MOT laser beams. On either side at the end of the cylindric chambers are two viewports, one for the MOT laser and the second one can optionally be used for excitation lasers, CCD cameras etc. Furthermore, the flanges for connecting the chamber to the TSR (Testspeicherring) are located at these ends as well. The horizontal cold lithium beam is entering the main chamber from the 2D-MOT chamber perpendicular to the symmetry axis of the spectrometer. The 2D-MOT chamber is connected to the main chamber by a tube with a length of 8 cm and a diameter of 6 mm to enable differential pumping. Thus, a pressure of 10^{-9} mbar in the main chamber were obtained with the 2D-MOT and the oven in operation, even before baking out the main vacuum chamber.

4.3 The Magneto-Optical Trap

4.3.1 The Magnetic Field of the MOT

The challenge of designing a MOT that can be combined with a Remi lies in the incompatibility of the magnetic quadrupole field of the MOT with the homogeneous

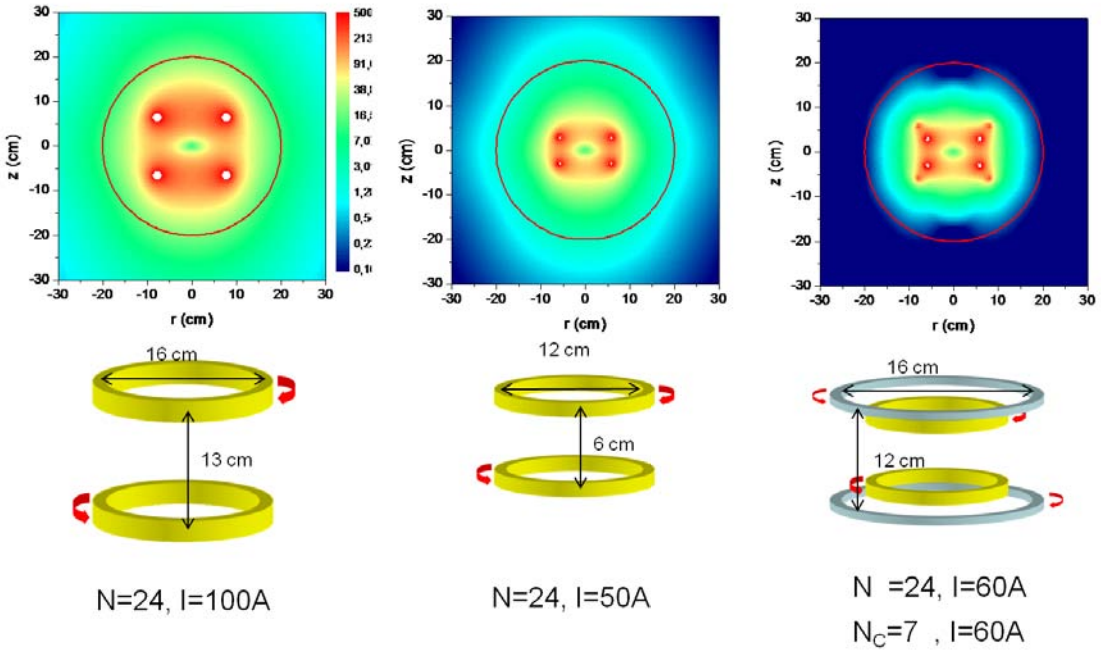

Figure 4.3: Magnetic field strengths for different coil setups: In the upper part, the density plots show the absolute magnetic field strengths in gauss dependent on the axial and radial distances to the center. The red circle depicts the chamber wall. In the lower part, the coil setups generating the respective fields are shown. The red arrows denote the directions of the current. N: Number of windings, N_c: Number of windings of the compensation coils (grey circles)

magnetic field of the Remi. Thus, the MOT needs to be switched off for electrons to be measured. The switching induces Eddy currents which in turn induce magnetic fields that make the electrons' measurement impossible until they disappear, see Fig. 4.1. As already mentioned in section 4.1.2, minimizing the waiting period is important to maintain a sufficient target density and to ensure short duty cyles, therefore Eddy currents need to be minimal.

In order to reduce Eddy currents, the magnetic flux through the metal chamber walls has to be minimized. However, the gradient in the center of the MOT needs to remain unchanged. Therefore the setup of the coils, which generate the magnetic field, has been customized based on simulations, see Fig. 4.3. The first column shows a scheme of the setup that was used by Schuricke et al. [Sch08], (see also Fig. 4.1,) and a simulation of the magnetic field. The coils have 24 windings each, a diameter of 16 cm and a distance of 13 cm. The first improvement, shown in the second column, is the reduction of the distance of the coils to 6 cm and of their diameter to 12 cm and the reduction of the current by 50 %, which already leads to

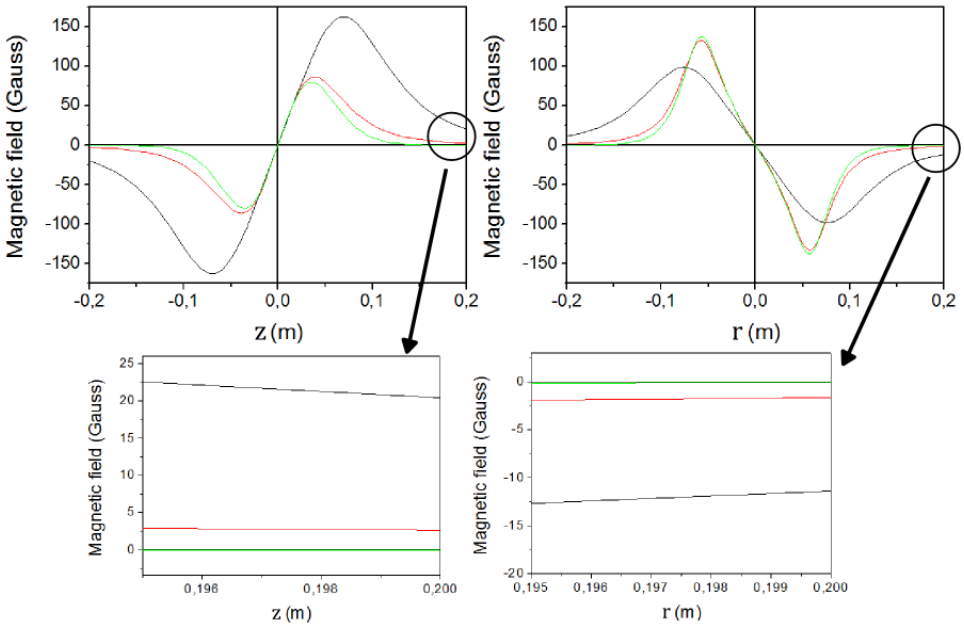

Figure 4.4: Magnetic field strength in axial and radial direction of the MOT: The chamber walls are located at -0.2 m and at 0.2 m. Black line: field strength of 'big' coils, red line: compact coils, green line: compact coils and compensation coils, see Fig. 4.3.

a reduction of the outer field. The gradient in the center is unchanged. The second step, shown in the third column, is the addition of a pair of compensation coils, which frames the MOT coils. The coils have a radius of 16 cm and a distance of 12 cm, but only 7 windings. They have opposite currents with respect to the inner pair of coils. Thus, they generate a magnetic field, which partially compensates the field of the inner coils. With a 20 % higher current, compared to the setup with one pair of compact coils, the inner gradient is the same, but the outer field is strongly reduced. The setup with compensation coils, which has been chosen for the experiment, leads to a field strength less than 0.3 gauss within the chamber walls with a current of 60 A, which is a reduction of the magnetic field strength within the chamber walls by a factor of 100, which is sufficient for the experiment.

The switching of the magnetic field has also been optimized. After the current through the MOT coils is switched off, a short pulse of opposite current induces a magnetic field that leads to a faster decreasing of the original field.
The setup of the coils and the switching was tested with a test version of the coils surrounded with metal. The measurement wit a Hall probe showed that the reduction of the magnetic flux through the chamber walls and the switching method lead

to a time of 200 μs, in which the magnetic field disappears.

Present Status of the MOT

The setup of the MOT has been built and the MOT is implemented into the spectrometer (see section 4.4). So far, the MOT is not operated and the laser setting is still in progress.

4.4 The Remi

There are two possible directions for the projectile beam, perpendicular to the direction of extraction or almost parallel. The parallel setup enables measuring of electrons, which are emitted in the projectile's direction with a significantly higher energy than other electrons have, i.e. energies of a few keV, and which are emitted in special classes of experiments, ECC (non-radiative electron capture to the continuum), ELC (electron loss to the continuum), RECC (radiative electron capture to the continuum) [UMD+03a]. However, the projectile beam limits the space for the detectors, which is not the case for the perpendicular setup, with which the mentioned electrons cannot be detected. In order to detect the fast electrons, the parallel setup was chosen. A scheme of the spectrometer is depicted in Fig. 4.5. The spectrometer has a total length of 85 cm and a maximal width of 19 cm. It consists of coaxial aluminium rings, which are cut in order to reduce Eddy currents. They are connected by electric resistors. The voltage can be applied on several rings so that different configurations of the spectrometer can be realized, e.g. time focusing by setting a drift region with double the length of the acceleration region and electric lenses. The ion side of the spetrometer has 11 diffrent connections, the electron side has 7 connetions.

The usual cylindrical shape of a spectrometer of a Remi could not be used in this special case. Since the MOT was designed in a very compact way in order to reduce the magnetic flux through the chamber walls (see section 4.3.1), the coils could not be positioned outside the spectrometer. They could also not be positioned inside, since they would influence the electric extraction field. Thus the coils needed to be integrated into the spectrometer by making the coil holders part of the spectrometer rings. Hence the spectrometer has a diameter of 12 cm in the center. The

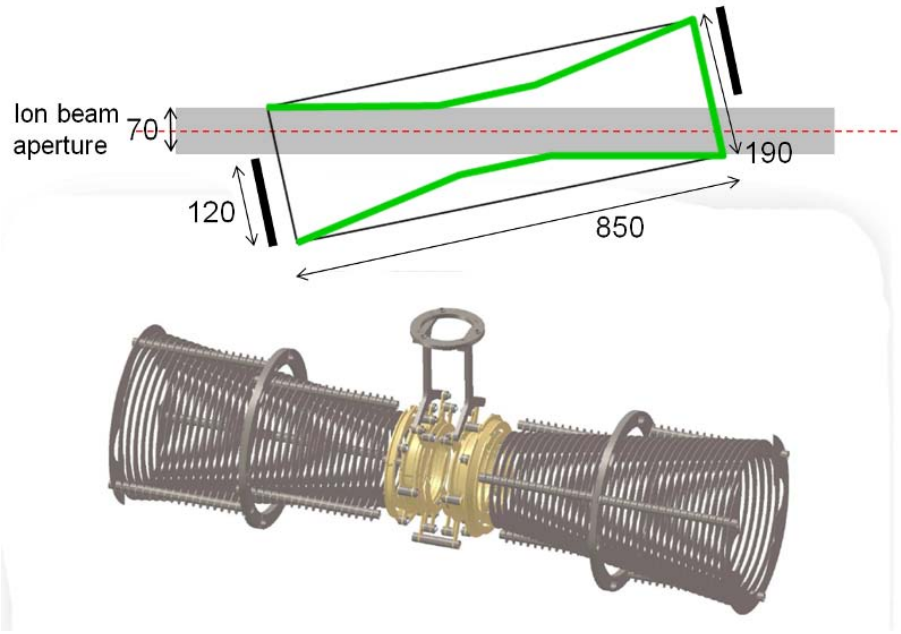

Figure 4.5: The spectrometer of the MOTRemi: Upper part: A scheme deepicting the way of the projectile ion beam through the spectrometer. Lower part: Technical drawing of the spectrometer: In gold: the holding structure of the MOT coils integrated into the spectrometer, in grey: The trumpet-shaped spectrometer and the suspension of the MOT coils.

projectile ion beam has to cross the chamber under an angle of 8° with respect to the spectrometer's symmetry axis so that it does not hit the detectors. Further, an aperture of at least 7 cm is needed for the beam before cooling, since the beam is then broader and has different trajectories than the cooled beam. With a sufficient length of the spectrometer, this is geometrically not possible with a cylindric shape with a diameter of 12 cm. Thus, the spectrometer is trumpet-shaped and the detectors are initially positioned outside the spectrometer and can be moved in when the ion beam is cooled and collimated. For the implementation into the TSR, the whole chamber, which contains the spectrometer and the MOT, is tilted by 8° so that the ion beam passes through the spectrometer under the necessary angle. The ion and electron detectors are spatially resolved detectors consisting of a multi-channel plate and a delay line anode. They are capable of detecting simultaneous hits with a spatial distance of about 14 mm. For closer hits, a dead time of about 6 ns has to be taken into account. A test of the detector yielded a spatial resolution of $0.69 \pm 0.25\,mm$ in x-direction and of $0.64 \pm 0.24\,mm$ in y-direction. Due to limitations of the testing method, the measured resolutions are just upper limits, for further details see [Sel10].

4.5 The 2D-MOT as a Cold Lithium Source

A 2D-MOT as a source for cold lithium atoms has been first realized by Tiecke et al. [TGLW09]. This method was chosen over the Zeeman slower due to the collimated atom beam, since the distance from the slowing device to the MOT is at least 40 cm due to the diameter of the spherical part of the main chamber, which gives rise to a large divergence of the atom beam of a Zeeman slower. This would lead to a comparatively bad loading rate, since only a fraction of the beam would pass through the trapping region of the MOT.
The setup of the 2D-MOT is ideal to maintain good vacuum conditions in the main chamber, since the connection to the oven is perpendicular to the direction of extraction towards the MOT in the main chamber. Furthermore, the cold atomic beam of the 2D-MOT alone can already be used as a target, since its temperature is in the range of supersonic gas jets, or even below it.

4.5.1 The Oven

The oven is a cylinder with 47 mm inner diameter and a height of 25 mm, in which the lithium is melted. It is connected to the 2D-MOT chamber over a tube with 16 mm inner diameter and with a total length of 70 mm. It is heated by heating wire. The temperature is controlled by a thermocouple. When the source is operated, the oven is heated to a temperature of 350°C, which is well above the melting point of lithium.

4.5.2 The 2D-MOT Laser Properties

Both cooling and repumping lasers are detuned by $7.5\,\Gamma$ and have a power of 20 mW each. The beams have a diameter of 2 cm and intersect in the center of the 2D-MOT coils. The push beam drives the same transition as the repumping beam and has a power of 3 mW. With a saturation intensity I_S of ^{7}Li of 2.56 $\frac{mW}{cm^2}$, the saturation parameter is $s_0 = 7.8$ which is sufficient for laser cooling.

4.5.3 The Magnetic Field of the 2D-MOT

The two-dimensional magnetic field is created by four race-track coils, where two parallel pairs are orthogonally aranged as depicted in Fig. 4.6. Each coil has a current in opposite direction with respect to the adjacent coils. The coils are inside

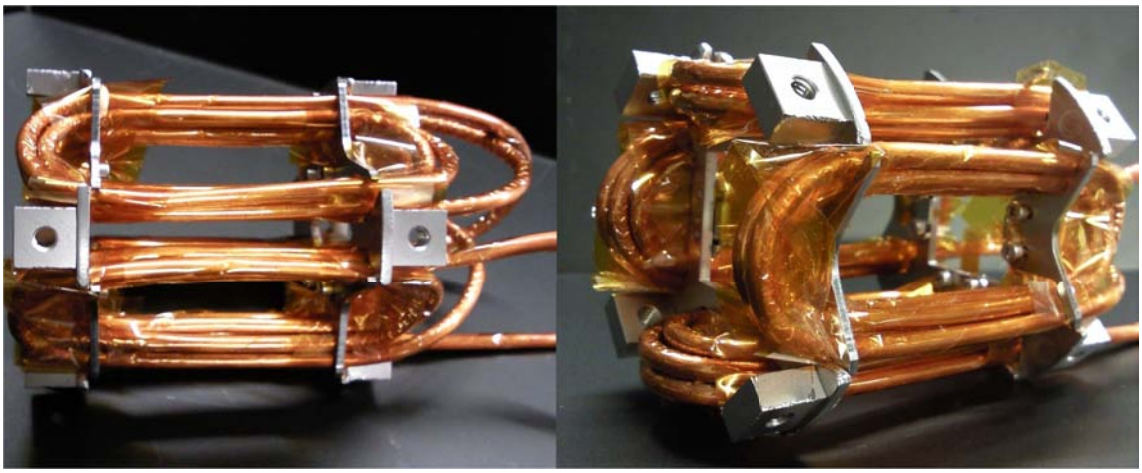

Figure 4.6: The race-track coils of the 2D-MOT: One can see the Kapton foil, which has additionally been wrapped around the coils where they are held by the aluminium structure, in order to prevent the holder from cutting through the insulation.

the vacuum, so that the required field gradient of at least 50 gauss/cm [TGLW09] can be achieved with a spatial small magnetic field that also has a smaller maximal field strength. This reduces the magnetic flow through the chamber walls, and thereby the Eddy currents when the field is switched off. The coils are operated at a current of about 60 A. Since they are in the vacuum, they cannot lose enough temperature by exchanging energy with the surrounding system and therefore need additional cooling. Thus, the coils are built of one copper tube, which has 2 mm inner and 3 mm outer diameter, and are water-cooled. They are insulated by Kapton foil, which is wrapped around the tube. Kapton does not outgas and is resistant to temperatures up to 670 K, which is important in order to withstand the temperature of the coils in operation and the baking of the whole vacuum system.
Fig. 4.7 shows the magnetic field of the coils at a current of 5 A in comparison to a simulation (based on a Mathematica notebook [ntcmf]) of a field which is generated by rectangular coils with the same dimensions. The measured data are in good agreement with the simulation. Thus, the magnetic field strength can be calculated for different currents.

The setup of the 2D-MOT is shown in Fig. 4.9. It has already been tested, see chapter 5. Fig. 4.8 shows a picture of the fluorescing atoms trapped within the 2D-MOT.

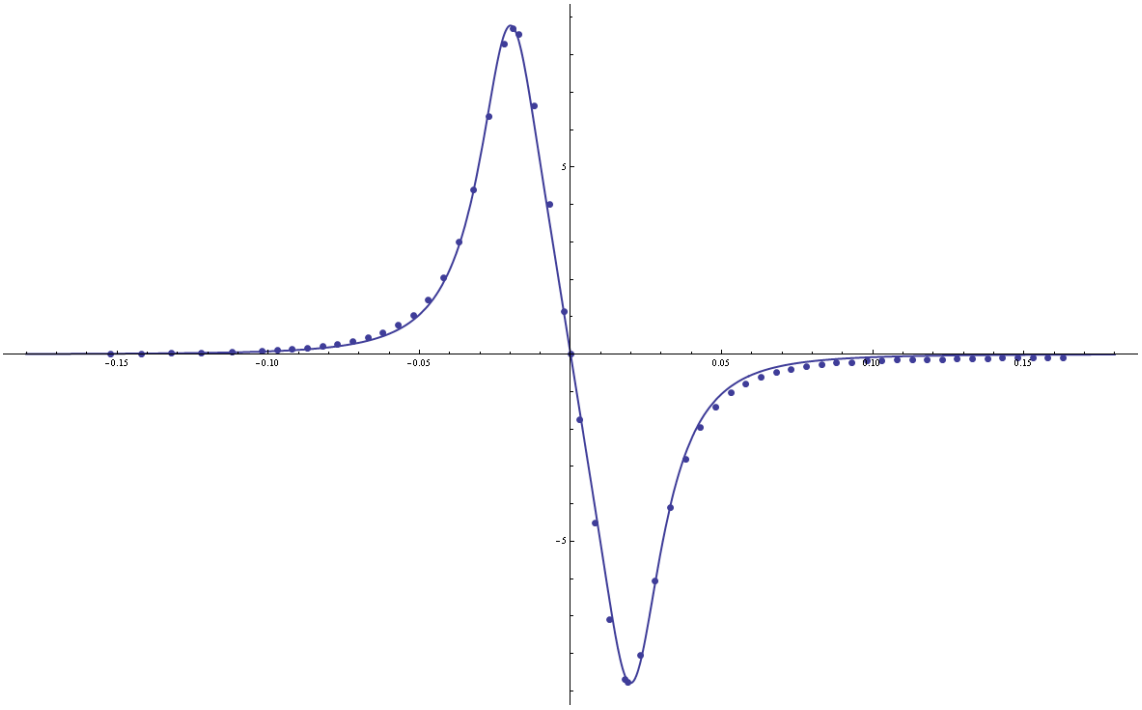

Figure 4.7: The magnetic field of the 2D-MOT at a current of 5 A: Dots: Measured data, continuous line: Simulation

4.6 The Laser System

The laser setup is depicted in Fig. 4.10. The laser system is powered by one commercially available TA laser, Toptica TA pro. It has a wave length of 671 nm and an output power of about 400 mW. The laser frequency is locked on the cross over signal of the D2-transition, an artifact resonance that occurs at Doppler-free spectroscopy. The signal for locking the laser is obtained in a spectroscopy cell. The laser beam is split into two beams which are shifted by AOMs to the transition frequencies of the D2-transition with an additional red-detunig of 7.5 Γ. Each beam is then split and guided by optics towards the coupling into optical fibres leading towards MOT and 2D-MOT. After the fibres, the beams are circular polarized by quarter-wave plates. At present, the setup for the 2D-MOT is finished and the MOT will be finished soon.

4.7 Experimental Cycle

A scheme of the planned experimental cycle is depicted in Fig. 4.11. In the first phase, the MOT is loaded. The 2D-MOT transversally cools the hot atoms emerging

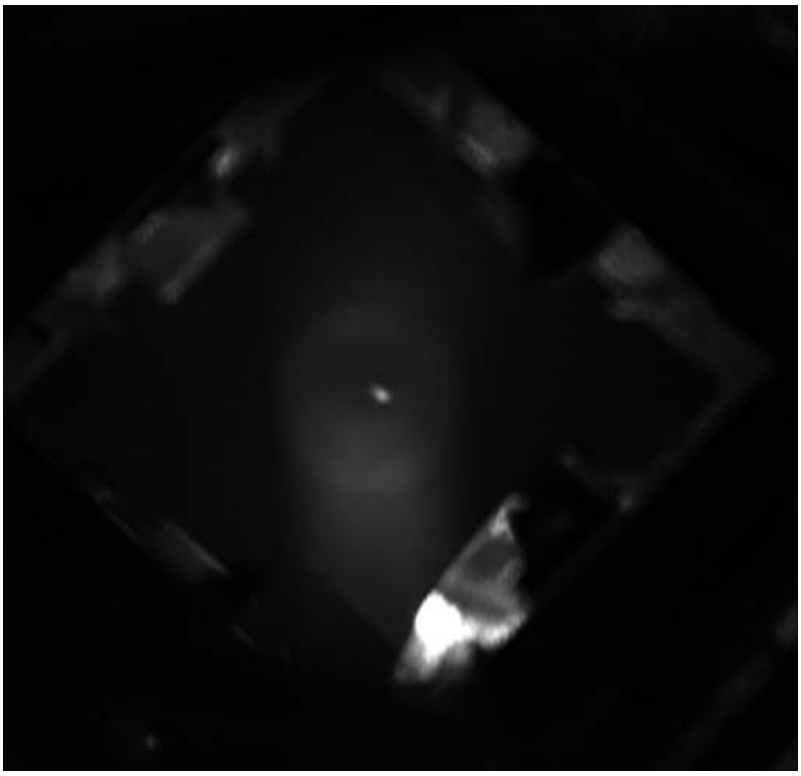

Figure 4.8: Picture of the 2D-MOT taken by a CCD camera: The picture is taken in axial direction. The bright spot in the center shows fluorescing temporarily trapped atoms. The bright area in the lower right corner is due to reflections of the laser on the coils.

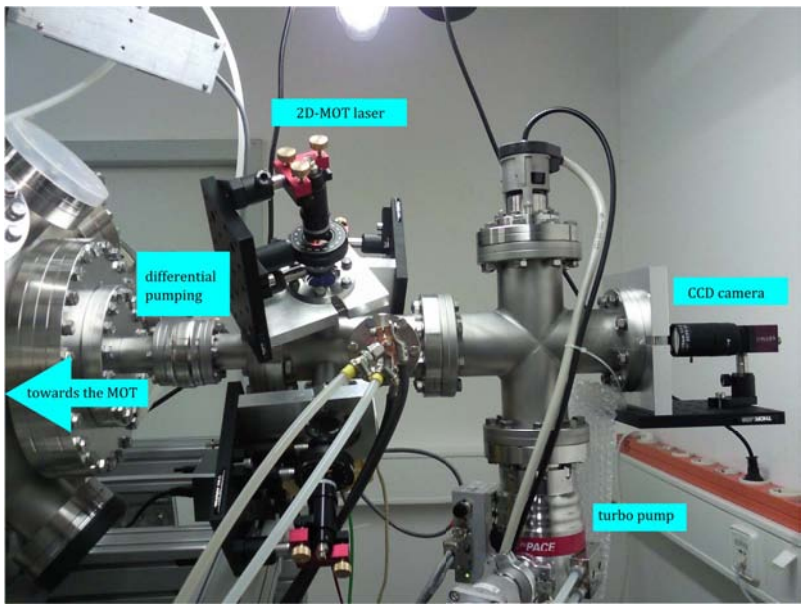

Figure 4.9: The setup of the 2D-MOT connected to the main vacuum chamber

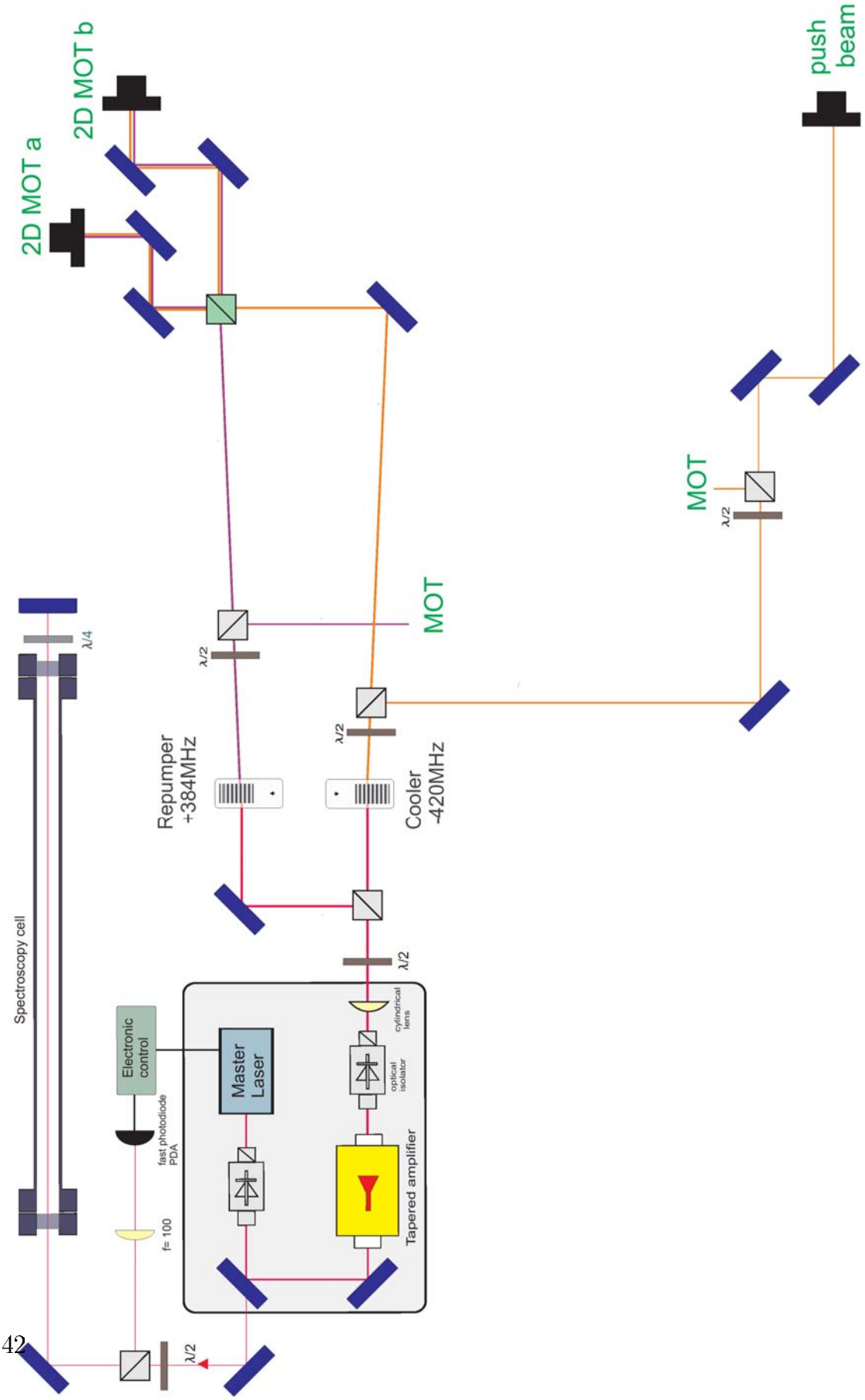

Figure 4.10: Laser system

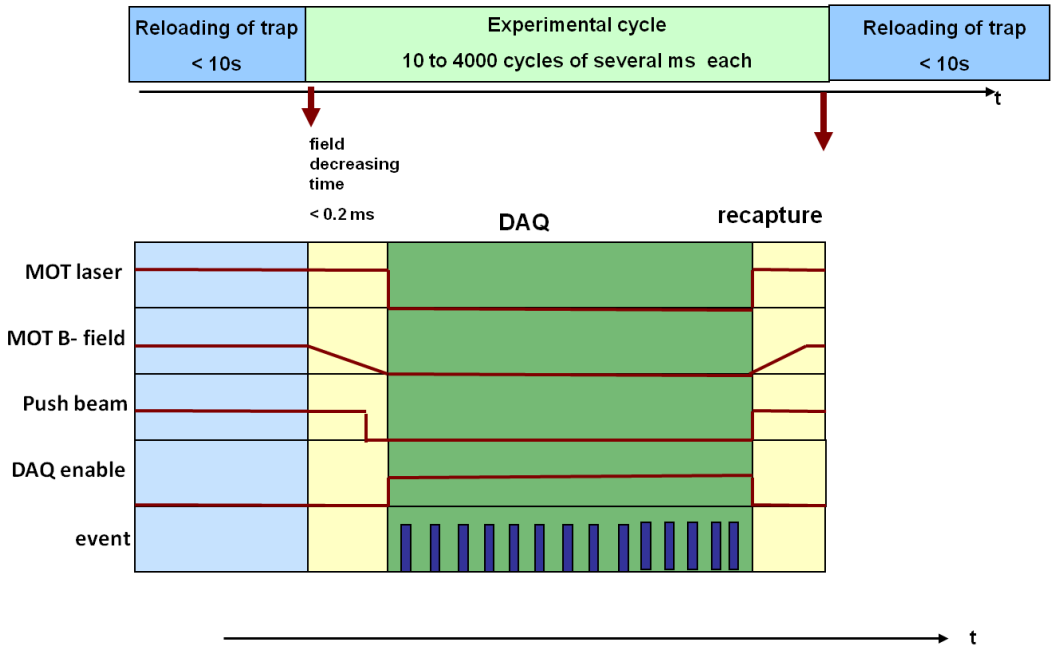

Figure 4.11: Scheme of the experimental cycle

from the lithium oven. The push beam transfers the cooled atoms towards the target MOT where they are recaptured. The loading time is estimated to be less than 10 s. In the second phase, the magnetic MOT field and the 2D-MOT are switched off. The MOT field disappears within 0.2 ms, while the push laser is switched off delayed in order to steer the remaining atoms on the way towards the MOT. The MOT lasers are still in operation and create an optical molasses thereby slowing the diffusion of the prior trapped atoms out of the reaction volume. In the third phase, the data acquisition is enabled. MOT and 2D-MOT are completely switched off. The reaction volume is exposed to the projectile beam and the ionization events are measured for a few ms, then the remaining target atoms have to be recaptured before they diffuse to far. In the fourth phase, the atoms that remained in the trapping region are reaptured in the MOT, therefore the magnetic MOT field and the MOT lasers are switched on. The push laser is operated, too, in order to push atoms, which diffused out of the trapping region back to the trapping region. Phase two to four are repeated up to a few 1000 times until the target density is too low and reloading is necessary. Then the cycle starts with a new loading phase. The duty cycle is estimated to be 10 % to 50 % of the whole cycle.

5 Characterization of the 2D-MOT

5.1 Experimental Setup

The 2D-MOT will be used to load the target MOT with a cold atomic lithium beam. It is important to know the properties of the lithium beam in order to be able to estimate the loading rate of the target MOT. Therefore, the atoms in the lithium beam coming from the 2D-MOT are excited by a laser. Then a UV laser photo-ionizes the excited atoms. The recoil ions are measured with the ion spectrometer of the Remi. The width of the lithium beam and its temperature in its propagation direction can be determined from the ions' position spectrum.
The lithium is heated in an oven to a temperature of 350°C, the atoms emerging from the oven are transversally cooled in the 2D-MOT. The cooling and the repumping laser beams have a power of 20 mW each and they are red-detuned by $7.5\,\Gamma$, (Γ is the natural width of the excited state). The push laser has a power of 1 mW and the frequency of the repumping laser. The coils are operated at a current of 50 A. According to the simulation of the magnetic field this induces a field gradient of about 45 gauss/cm. The reaction volume is created by the overlap of the lithium beam, the excitation laser and the UV laser, see Fig. 5.1. The lithium beam enters the spectrometer perpendicular to the extraction field along the x-axis. The UV laser crosses the lithium beam with an angle of 18° with respect to the y-axis. It has a width of 1 mm in the x-y-plane and a width of 7 mm in the z-direction. The excitation laser crosses the other two beams where they intersect. It has a circular profile with a 20 mm diameter. The diameter of the excitation laser is chosen large enough for the whole overlap of the lithium beam and the UV laser to be illuminated. The ion detector lies in a plane parallel to the x-y-plane in z-direction.
The excitation laser has a power of 3 mW and the frequency of the cooling laser, since the push beam of the 2D-MOT has the frequency of the repumper and the atoms in the beam have been pumped into the dark state with respect to the repumper. The UV laser is a commercially available passively Q-switched frequency-quadrupole Nd:YAG laser. It is pulsed with a pulse width of 400 ps and has a wavelength of 266 nm,

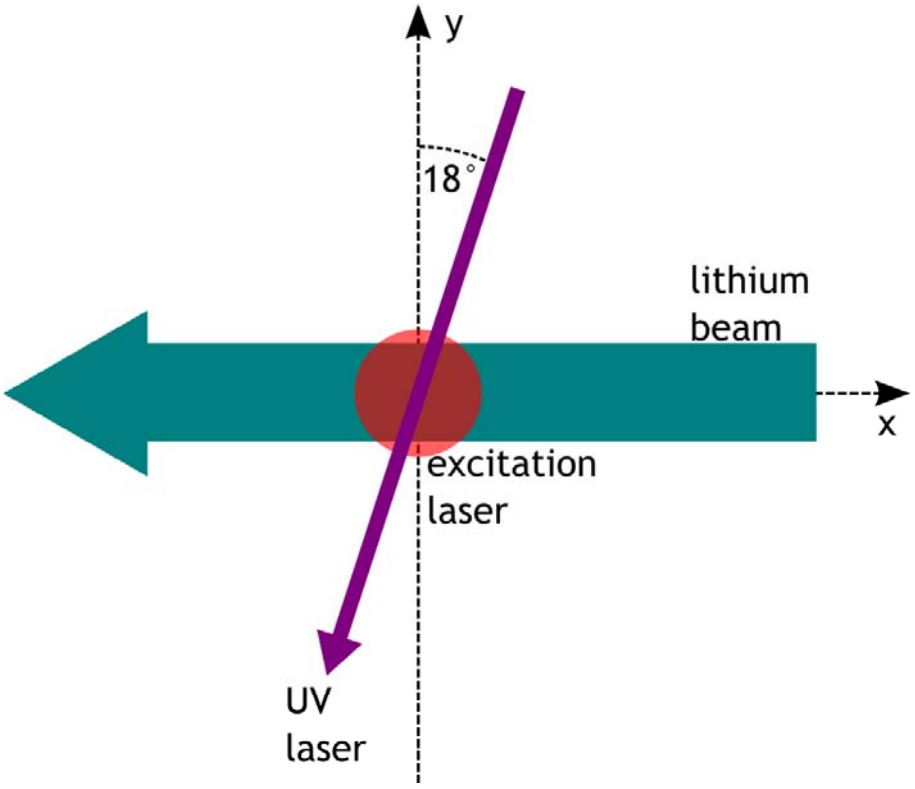

Figure 5.1: Scheme of the experiment

thus it only photo-ionizes the excited atoms.
The acceleration potential of the extraction field for the ions is set to a voltage of $U = 28\,V$ and the ratio of lengths of acceleration and drift region enables time focusing. The time of flight measurement is triggerd by the UV laser pulse upon its detection by a photo diode. The ions produced by the laser pulse can be identified by a peak in the time of flight spectrum, see Fig. 5.2. In order to reduce the background, only events of this time period are taken into account. The FWHM of the time of flight peak is 42 ns. However, the time resolution is a few ns. The width needs other explanations, since time focusing is enabled. The reaction volume has a longitudinal width of 7 mm with respect to the direction of extraction which is too large for the time focusing to work, thus the longitudinal starting position has an effect on the time of flight. Due to the SIMION simulation this would lead to a width of 10 ns. A larger effect, as SIMION simulations showed, is that the time of flight is dependent on the position in the transversal plane due to inhomogeneities of the electric extraction field which appear at the changeover from the extraction field to the field-free drift region. As one can see in Fig. 5.3 the electric field which

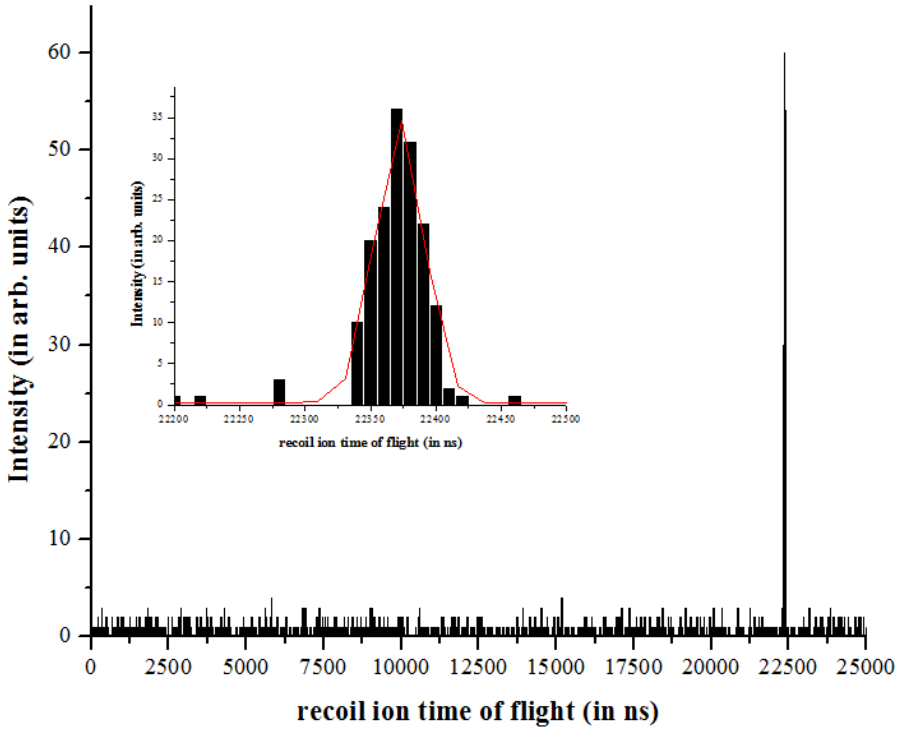

Figure 5.2: Time of flight spectrum of the recoil ions: The inset shows a zoom in on the peak with a gaussian fit.

an ion passes through differs in dependence of the transversal position.

5.2 Results and Discussion

Width of the Lithium Beam at the Center of the MOT

Fig. 5.4 shows the position spectrum of the recoil ions. One can clearly see a linear structure tilted by 18° with respect to the y-axis, which is the projection of the reaction volume on the detector. The width of the lithium beam can be estimated by the width of the peak in the position spectrum's projection to the y-axis and it is 17 mm.

The Temperature of the Lithium Beam

The spread of the lithium atoms' transversal momenta $\Delta p_\perp$, with respect to the ions' direction of extraction, can be calculated by the width d of the recoil ions' position spectrum, see Fig. 5.4. The width is determined by rotating the position

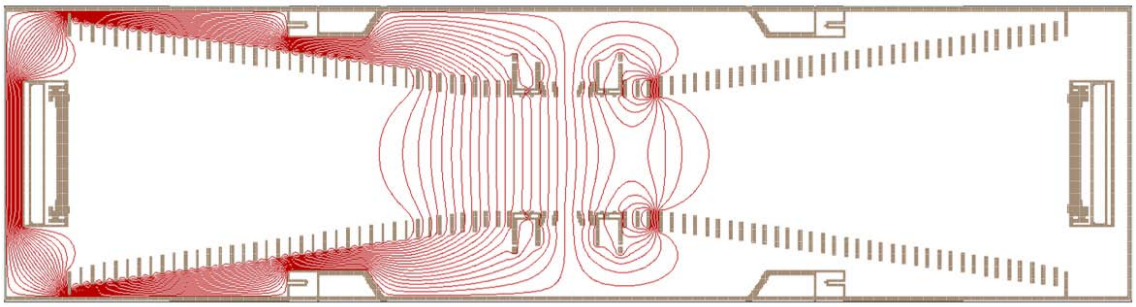

Figure 5.3: SIMION simulation of the electric field in the spectrometer for the used setup

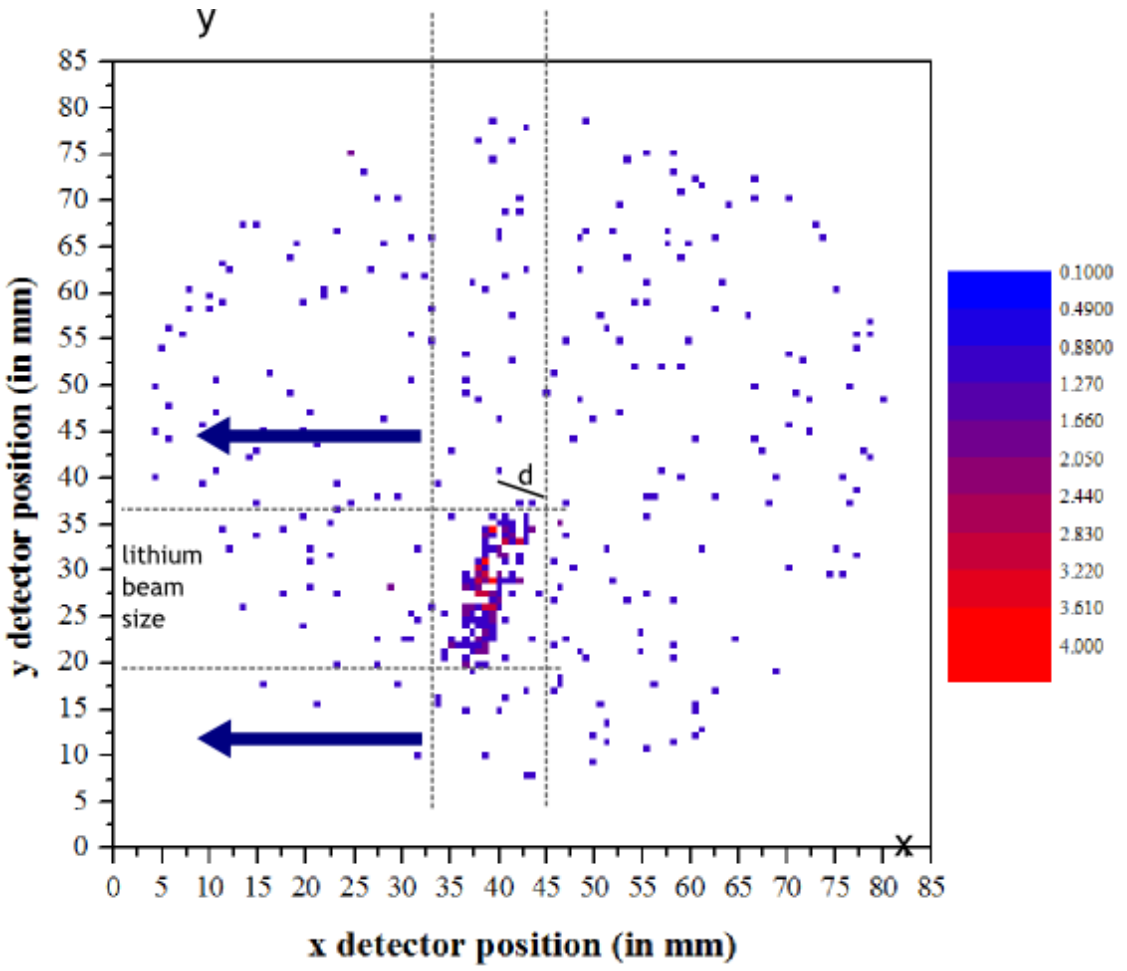

Figure 5.4: Position spectrum of the recoil ions: The vertical lines denote the background cutoff, only events between the lines are considered. The blue arrows depict the projection of the data to the y-axis.

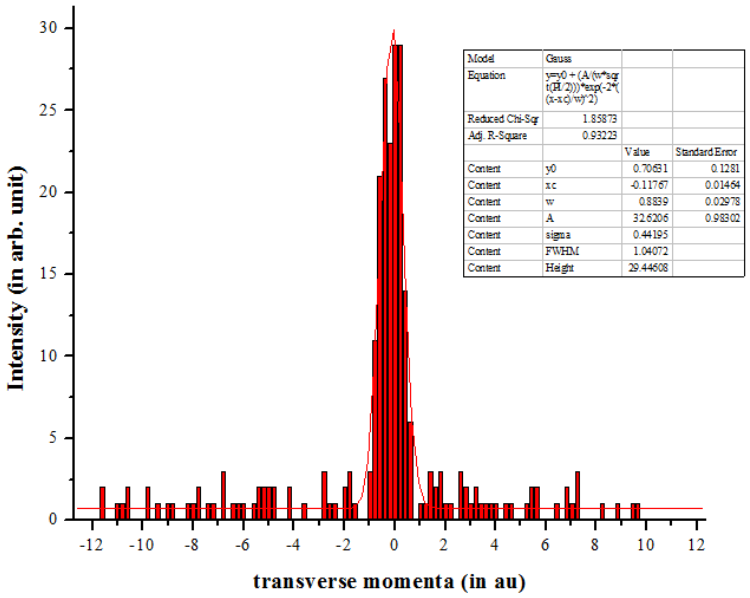

Figure 5.5: Transverse momentum relative to the mean transverse momentum

spectrum by 18° and projecting it to the x'-axis. $\Delta p_\perp$ in propagation direction of the lithium beam can be derived by using equation (3.6) with the distance R_r to the maximum of the peak and multiplying the result by $cos(18°)$, since the position spectrum was rotated. Thus one obtains the momentum spread relative to the mean momentum. The transversal temperature can be determined by fitting a Gaussian distribution on the data. The variance of this Gaussian distribution together with the one-dimensional Maxwell-Boltzmann-distribution leads to:

$$\sigma^2 = m_{Li} k_B T \Rightarrow T = \frac{\sigma^2}{m_{Li} k_B} \tag{5.1}$$

With $\sigma' = \sigma \cdot cos(18°) = cos(18°) \cdot 0.44\,au$ the transversal temperature is 4.3 K. The estimated temperature of the atoms is an upper limit, since the momentum transfer to the recoil ion is about 0.3 au by photo-ionization. Since σ of the measured ions' momentum distribution is 0.44 au and hence at the same scale as the momentum transfer, a considerable fraction of the ions' momentum spread is due to the ionization. Therefore, the atoms' temperature is lower than the calculated temperature. Further, a defocusing lens-effect of the electric extraction field due the changeover from the extraction field to the field-free drift region, see Fig. 5.3, causes a broadening of the position spectrum. Thus, the calculated momenta are too big. These effects can be considered in the calculations. However, this was not possible in the

time for this thesis.

Event Rate

The event rate is given by

$$R = \sigma \cdot \rho r \rho_{ee} \cdot N_\gamma \tag{5.2}$$

with the photo-ionization cross section σ, the atom density ρ, the length of the UV laser's path through the reaction volume r, the number of UV photons per second N_γ and the fraction of excited atoms ρ_{ee}. The energy of one pulse of the UV laser is specified by the manufacturer to be $0.7\,\mu$J, that corresponds to about 10^{12} photons per pulse. With a repetition rate of 9 kHz the number of photons per second is about $N_\gamma = 9 \cdot 10^{15}/s$. The atom density is calculated as follows:

$$\rho = \frac{\dot{n}}{A \cdot v} \tag{5.3}$$

$\dot{n}$ is the flux rate of atoms in the lithium beam, A the lithium beam's area and v the mean velocity of the atoms in the beam. The lithium beam has a diameter of 1.7 cm; assuming a flow rate of atoms from the 2D-MOT of $\dot{n} = 10^9/s$ and further a velocity of $v = 40\frac{m}{s}$, which is estimated according to the data by Tiecke et al. [TGLW09], a density of atoms in the beam of $\rho = 350000/cm^3$ is obtained. The fraction of excited atoms ρ_{ee} is calculated with equation (2.3). The power of the excitation laser is 3 mW. The intensity is about 1 $\frac{mW}{cm^2}$, the saturation intensity I_S of ^{7}Li is 2.56 $\frac{mW}{cm^2}$, thus the saturation parameter is $s_0 = 0.4$. The distance of the reaction volume is greater than 40 cm, the diameter of the lithium beam is 1.7 cm, thus the atoms' velocity transverse to the beam is less than $1\frac{m}{s}$. The detuning of the excitation laser is $\delta_0 = 7.5\Gamma$. Thus, the fraction of excited atoms is less than $1.42 \cdot 10^{-3}$. With the assumption that the cross section of the photo ionization is $\sigma \approx 6 \cdot 10^{-18} cm^2$, which is based on calculations of cross sections by Lahiri and Manson [LM93] and measurements by Wippel et al. [WBH+01], one achieves a rate of $R \approx 45\,Hz$. However, the actual rate was two events per minute, i.e. 0.03 Hz. This can have several reasons. Since the 2D-MOT is not optimized yet, the flux of atoms could be less than $10^9/s$. Further, the fraction of excited atoms could be less than calculated, since it was assumed that the atoms have a velocity of $1\frac{m}{s}$ opposing the excitation laser. A smaller velocity or a velocity in the other direction would set

the atom more off resonace and the fraction of excited atoms would be smaller.
For further tests, it is planned to focus the excitation laser into the intersection of the UV laser and the lithium beam in order to achieve a higher laser intensity in the reaction volume, thus higher event rates can be obtained. The focusing will also reduce the size of the reaction volume and therefore reduce the broadening of the time of fligth spectrum.

6 Conclusion

This diploma thesis was performed within a project where a magneto-optical trap reaction microscope (MOTRemi) was developed for the study of ion-atom collisions. In a MOTRemi the trapping and cooling of a magneto-optical trap (MOT) is combined with a momentum-imaging spectrometer for recoil ions and low-energetic electrons, a so-called Reaction Microscope (Remi). By laser cooling, one obtains target temperatures of a few hundred microkelvin, more than two orders of magnitude lower than in conventional supersonic gas jets, leading up to about a factor of 10 greater momentum resolution compared to other reaction microscopes. Furthermore, a MOT can provide lithium, a new target for ion-atom collision experiments and a relatively simple atom. The setup developed in the PRIOC (**Pr**ecision studies on **I**on **C**ollisions) project might be the first reaction microscope with a MOT target that will enable the coincident detection of electrons and recoil ions.

The primary goal of this diploma thesis was the development of a source of cold lithium atoms to load the MOT. For this purpose, a 2D-MOT was developed that provides a cold atomic beam. In order to characterize some properties of this atom source, a first experiment was perfomed where the lithium atoms were ionized with a UV laser. The recoil ions were detected in the reaction microscope. Based on that measurement we estimate the temperature in longitudinal direction to be less than 4 K which already is at the scale of a supersonic gas jet. Thus, the temperature is sufficient for the atomic beam to be used as a stand-alone target.

The atomic flux, which has been achieved so far, can only be roughly estimated based on the ionization rate. Since the actual event rate is two orders of magnitude smaller than calculated, it is very likely that the assumed and aimed for flux of 10^9 atoms/s has not been gained yet. The full experimental optimization of the flux could not be performed in the framework of this thesis, because many diagnostic tools were not yet installed and available at the time (e.g. fluorescence imaging of the 2D-MOT and loading rate measurements of the 3D-MOT). The optimizations are currently under way and will be finished in the next weeks.

At present the whole MOTRemi setup is prepared to be implemented into the TSR (Testspeicherring). The first beam-time and commissioning is scheduled for this summer. It will be possible for the first time to perform kinematically complete ion-atom collision measurements with a lithium target, which will help to solve the discrepancies between earlier theoretical and experimental results.

Part I

Appendix

A Lists

A.1 List of Figures

B Bibliography

[Bet30] H. Bethe. Zur theorie des durchgangs schneller korpuskularstrahlen durch materie. *Annalen der Physik*, 5:325–400, 1930.

[BFC+08] J. Blieck, X. Fléchard, A. Cassimi, H. Gilles, S. Girard, and D. Hennecart. A new motrims apparatus for high resolution measurements in ion-atom collisions and trapped atoms studies. *Review of Scientific Iinstruments*, 79:103102, 2008.

[DNS07] M Dürr, B. Najjari, and M. Schulz. Analysis of experimental data for ion-impact single ionization of helium with monte carlo event generators based on quantum theory. *Physial Review A*, 75(062708), 2007.

[egc] Neg: Non evaporable getter coating. http://est-div-sm.web.cern.ch/est-div-sm/project-getter-home.htm.

[Fis03] D. Fischer. *Mehr-Teilchen-Dynamik in der Einfach- und Doppelionisation von Helium durch geladene Projektile.* PhD thesis, Ruprecht-Karls-Universität Heidelberg, 2003.

[FMS+03] D. Fischer, R. Moshammer, M. Schulz, A.B. Voitkiv, and J. Ullrich. Fully differential cross sections for the single ionization of helium by ion impact. *Journal of Physics B*, 36(3555), 2003.

[FO04] J. Fiol and R.E. Olson. Three- and four-body dynamics in fast heavy ion-atom ionization. *Journal of Physics B*, 37(3947), 2004.

[Foo05] C.J. Foot. *Atomic Physics.* Oxford University Press, 2005.

[FOO06] J. Fiol, S. Otranto, and R.E. Olson. Critical comparison between theory and experiment for c^{6+}+he fully differential ionization cross sections. *Journal of Physics B*, 39(L285), 2006.

[LM93] J. Lahiri and S.T. Manson. Radiative recombination and excited-state photoionization of lithium. *Physical Review A*, 48(3674), 1993.

[MAM+10] M. McGovern, D. Assafrao, J.R. Mohallem, C.T. Whelan, and H.R.J. Walters. Coincidence studies of he ionized by c^{6+}, au^{24+}, and au^{53+}. *Physical Review A*, 81:042704, 2010.

[MvdS99] H.J. Metcalf and P. van der Straten. *Laser Cooling and Trapping*. Springer, 1999.

[ntcmf] Mathematica notebook to calculate magnetic fields. http://www.phy.duke.edu/research/photon/qoptics/techdocs/tools/coils.nb.

[RBIM99] T.N. Rescigno, M. Baertschy, W.A. Isaacs, and C.W. McCurdy. Collisional breakup in a quantum system of three charged particles. *Science*, 286(5449):2474, 1999.

[RJJ63] M.E. Rudd and T. Jorgensen Jr. Energy and angular distribution of electrons ejected from hydrogen and helium gas by protons. *Physical Review*, 131:1463–1545, 1963.

[Rut11] E. Rutherford. The scattering of α and β particles by matter and the structure of the atom. *Philosophical Magazine*, 21:669–688, 1911.

[Sch08] M. Schuricke. Multiphoton ionization of lithium, 2008.

[SDN+07] M. Schulz, M. Dürr, B. Najjari, R. Moshammer, and J. Ullrich. Reconciliation of measured fully differential single ionization data with the first born approximation convoluted with elastic scattering. *Physical Review A*, 76(032712), 2007.

[Sel10] M. Sell. Entwicklung, Aufbau und Test eines ortsempfindlichen Teilchendetektors zur Untersuchung von Stössen zwischen Ionen und lasergekühlten Atomen, 2010.

[SK05] C.A. Stan and W. Ketterle. Multiple species atom source for laser-cooling experiments. *Review of Scientific Iinstruments*, 76:063113, 2005.

[SMM+01] M. Schulz, R. Moshammer, D.H. Madison, R.E. Olson, P. Marchalant, C.T. Whelan, H.R.J. Walters, S. Jones, M. Foster, H. Kollmus, A. Cassimi, and J. Ullrich. Triply differential single ionization cross sections in coplanar and non-coplanar geometry for fast heavy ion-atom collisions. *Journal of Physics B*, 34:L305, 2001.

[Ste07] J. Steinmann. *Multiphoton Ionization of Laser Cooled Lithium*. PhD thesis, Ruprecht-Karls-Universität Heidelberg, 2007.

[SVH05] C. Slowe, L. Vernac, and L.V. Hau. High flux source of cold rubidium atoms. *Review of Scientific Iinstruments*, 76:103101, 2005.

[TGLW09] T.G. Tiecke, S.D. Gensemer, A. Ludewig, and J.T.M. Walraven. A high-flux 2d mot source for cold lithium atoms. *Physical Review A*, 80(013409), 2009.

[THK+01] J.W. Turkstra, R. Hoekstra, S. Knoop, D. Meyer, R. Morgenstern, and R.E. Olson. Recoil momentum spectroscopy of highly charged ion collisions on magneto-optically trapped na. *Physical Review Letters*, 87:123202, 2001.

[UMD+97] J. Ullrich, R. Moshammer, R. Dörner, O. Jagutzki, V. Mergel, H. Schmidt-Böcking, and L. Spielberger. Recoil-ion momentum spectroscopy. *Journal of Physics B*, 30:2917–2974, 1997.

[UMD+03a] J. Ullrich, R. Moshammer, A. Dorn, R. Dörner, L. Ph. H. Schmidt, and H. Schmidt-Böcking. Recoil-ion and electron momentum spectroscopy: reaction-microscopes. *Reports on Progress in Physics*, 66:1463, 2003.

[UMD+03b] J. Ullrich, R. Moshammer, A. Dorn, R. Dörner, L.Ph.H. Schmidt, and H. Schmidt-Böcking. Three-dimensional imaging of atomic four-body processes. *Nature*, 422:48–50, 2003.

[vdPNGA01] M. van der Poel, C.V. Nielsen, M.-A. Gearba, and N. Andersen. Fraunhofer diffraction of atomic matter waves: Electron transfer studies with a laser cooled target. *Physical Review Letters*, 87:123201, 2001.

[WBH+01] V. Wippel, C. Binder, W. Huber, L. Windholz, M. Allegrini, F. Fuso, and E. Arimondo. Photoionization cross-sections of the first excited states of sodium and lithium in a magneto-optical trap. *The European Physical Journal D*, 17:285–291, 2001.

Erklärung:

Ich versichere, dass ich diese Arbeit selbstständig verfasst habe und keine anderen als die angegebenen Quellen und Hilfsmittel benutzt habe.

Heidelberg, den (Datum) .....